AN AUTOMATED TETHER MANAGEMENT SYSTEM FOR EXTRAVEHICULAR ACTIVITIES IN MICROGRAVITY

by

Christopher Robin Hirschi

A thesis submitted to the faculty of
The University of Utah
in partial fulfillment of the requirements for the degree of

Master of Science

Department of Mechanical Engineering

The University of Utah

December 2003

THE UNIVERSITY OF UTAH GRADUATE SCHOOL

SUPERVISORY COMMITTEE APPROVAL

of a thesis submitted by

Christopher Robin Hirschi

This thesis has been read by each member of the following supervisory committee and by majority vote has been found to be satisfactory.

_____	_____
	Chair: Mark A. Minor
_____	_____
	Sanford G. Meek
_____	_____
	William K. VanMoorhem

THE UNIVERSITY OF UTAH GRADUATE SCHOOL

FINAL READING APPROVAL

To the Graduate Council of the University of Utah:

I have read the thesis of Christopher Robin Hirschi in its final form and have found that (1) its format, citations, and bibliographic style are consistent and acceptable; (2) its illustrative materials including figures, tables, and charts are in place; and (3) the final manuscript is satisfactory to the supervisory committee and is ready for submission to The Graduate School.

Date	Mark A. Minor Chair: Supervisory Committee

Approved for the Major Department

Joseph C. Klewicki
Chair

Approved for the Graduate Council

David S. Chapman
Dean of The Graduate School

ABSTRACT

When engaged in extravehicular activity (EVA) in the microgravity of space, safety requires astronauts to employ multiple tethers to ensure proximity of their person and tools to the spacecraft. Due to the cumbersome nature of constant tethering activities, this necessary component of EVA consumes a large amount of highly valuable time. This research investigates an automated system for the simplification of tether use.

The automated tether management system consists of a remotely releasable robotic gripper that secures the system to the spacecraft, a retractor that contains and controls the length of extended tether, and a hybrid tether that provides both tensile structural support and communication between the gripper and retractor. The gripper is optimized to engage a variety of anchor types and is self-locking. The retractor employs active as well as passive retraction capability that minimizes consumption of power.

Dynamic models are developed that simulate the system in reference frames that are fixed and in orbit in order to understand the limitations of the designed system and the effects of orbital dynamics. Experimentation and testing of the prototype system is described. Experiments measure key capabilities of each device, reveal unexpected characteristics of the system, and verify applicable dynamic simulations of the system. Expanded applications for the system outside the strict role of an astronaut safety tether are also considered.

This work is dedicated to my Julianne and my Tren, whose support and love have brought it to pass.

TABLE OF CONTENTS

LIST OF FIGURES

Figure

LIST OF SYMBOLS

B Viscous damping coefficient

d Center-to-center horizontal distance between pivot joints on coupler link that links gripper jaws to the lead screw nut

D Maximum travel of gripper lead screw nut

DOF Degree(s) of Freedom

d_{teth} Outer diameter of tether

EVA ExtraVehicular Activity

$\hat{e}_1$ Unit vector of orbital coordinate system describing direction of $\overline{r}_c$

$\hat{e}_2$ Unit vector of orbital coordinate system describing secondary in-plane direction orthogonal to $\hat{e}_1$

$\hat{e}_3$ Unit vector of orbital coordinate system describing out-of-plane motion, $\hat{e}_3 = \hat{e}_1 \times \hat{e}_2$

$\hat{e}_{1,A}, \hat{e}_{2,A}$ Unit vectors describing reference frame of astronaut in orbit

F Cost function minimized for gripper coupler link optimization

f_i Minimization term for anchors used in gripper linkage optimization

F_{jaw} Maximum force applied by gripper jaws to an anchor

$\overline{F}_{nc}$ Nonconservative force

F_{nut} Linear force exerted by the gripper leadscrew nut

G Universal gravitation constant

g_{eff} Acceleration due to gravity at altitude of astronaut

k Linear spring constant for approximation of retractor spring behavior

l Length of position vector $\overline{r}_1$

L Lagrangian

L_1 Center-to-center distance between pivot joints on coupler link that links gripper jaws to the lead screw nut

L_2 Center-to-center distance between pivot points on gripper jaws

J_g Moment of inertia of gripper about its center of mass

m_A Mass of astronaut

m_e Mass of the earth

m_g Mass of gripper

q_i ith generalized coordinate describing system dynamics

r Maximum moment arm of gripper jaws when engaging an anchor

$\overline{r}_{off}$ Vector describing offset in the gripper between its center of mass and the point of tether attachment

$\overline{r}_A$ Position vector locating the astronaut relative to the earth's center

$\overline{r}_c$ Position vector locating the gripper's center of mass relative to the retractor

$\overline{r}_G$ Position vector locating the gripper relative to the earth's center

$\overline{r}_j$ Vector describing the points of application of nonconservative forces

$\overline{r}_T$ Position vector locating attachment point of tether on gripper

r_0 Distance added to retractor spring extension to account for preload

$r_{1,A}, r_{2,A}$ Components of gripper position vector along corresponding unit vectors of orbital coordinate system

T Kinetic energy

V Potential energy

v_A Magnitude of astronaut's velocity relative to the earth's center of mass

V_{mot} Voltage applied to motor

W_i Optimization weighting factor for optimization parameter *i*

x Displacement of gripper lead screw nut from fully open position

x_0 Fully open position of gripper lead screw nut

X_{Fmag} Force magnification factor, ratio of the maximum force exerted by gripper jaws on an anchor to linear force exerted by the lead screw nut

α Transmission angle between gripper lead screw nut and coupler links

β .....Transmission angle between gripper coupler links and jaws

γ.....Generalized coordinate of orbital model reference system describing direction of $\overline{r}_c$ relative to $\overline{r}_A$

ε_{max} .....Maximum stress seen by the tether when wound on retractor reel

λ .....Angle of gripper jaw describing its position relative to vertical

λ_{toggle}.....Angle of gripper jaw defining toggle point with coupler link

λ_0.....Angle of gripper jaw relative to vertical in fully open position

ϕ .....Angle describing gripper's orientation in planar inertial coordinate frame

θ .....Direction of $\overline{r}_c$ in inertial polar coordinate frame

$\dot{\theta}_A$ .....Angular velocity of vector $\overline{r}_A$, which describes astronaut's position

ACKNOWLEDGMENTS

Special thanks to Mark Minor for design aid and indispensable guidance; those at NASA Johnson Space Center who made this work possible, including Robert Ambrose for the original research concept, Christopher Culbert, Dennis Wells, Scott Askew, Jennifer Rochlis, Ross Bentley, and Bobby Davis; and machinists Thomas Slowik and Jacob Scott for their dedicated work in a pinch that made gripper testing possible. NASA contracts NGT-9-54 and NAG 9-1422 are also greatly appreciated for partial support of this research.

1. INTRODUCTION

When engaged in Extravehicular Activity (EVA) in the microgravity of space, safety requires astronauts to employ multiple tethers to ensure the proximity of themselves and their tools to the spacecraft. In particular, it is required of astronauts to secure their person to the spacecraft with at least two safety tethers when stationary during EVA. This necessary component of EVA requires a significant amount of highly valuable time. Although documentation is not readily available regarding the full percentage of time spent managing tethers, a typical EVA egress procedure can involve 15 minutes of working with tethers to simply prepare to begin working. Doubling this time to account for reentering the spacecraft gives nearly 8% of a 6.5-hour EVA that is spent managing tethers only during exit from and reentry into the spacecraft [1].

Tethers that are in current use, such as the short waist tether (Figure 1a), consist of a flexible tensile structural member with manually operated hooks at each end. These hooks are specialized for manual operation, and are fastened around tether loops or cables that are integral to the equipment, suits, and structures with which the crewmembers interact. To allow a greater range of motion, the retractable safety tether (Figure 1b) is applied. This device features a spring-loaded reel that dispenses and controls the length of tether in the workspace. The safety tether can also engage slide wires (Figure 1c) that span the length of the Space Shuttle cargo bay to further expand the range of travel.

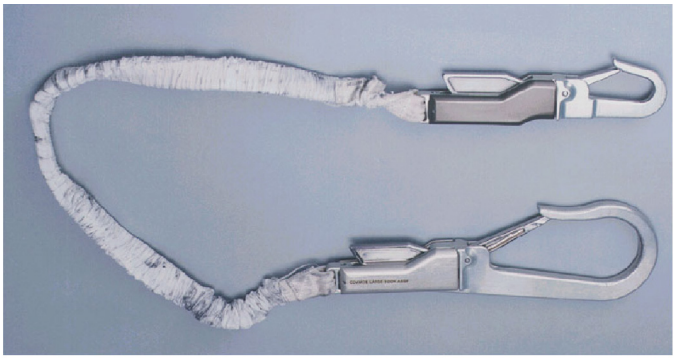

(a) Waist tether

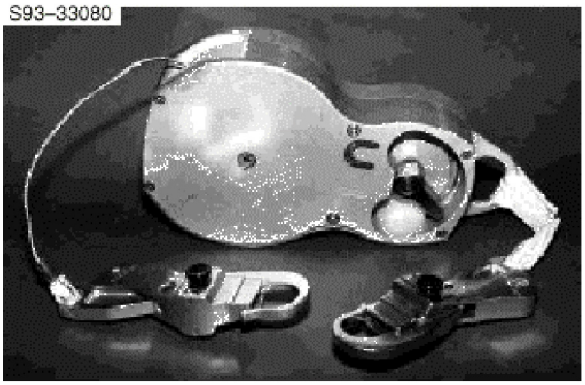

(b) Retractable safety tether

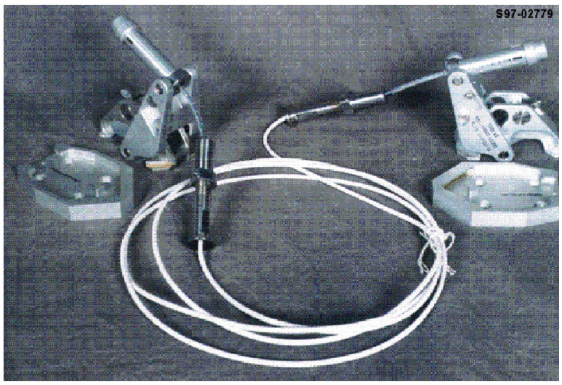

(c) Slide wire

Figure 1. Tethering devices in current use [2-4].

When complete, the International Space Station will be the largest spacecraft ever constructed, requiring many tether loops, slide wires, and handrails for tethered travel about its relatively large exterior. In order to travel past the range of one safety tether, an EVA crewmember would need to transfer his or her tether to a new anchor. Accomplishing this with currently used flight hardware would necessitate attaching a new tether to an anchor near the end of the current tether and returning to the initial anchor to release the first hook before continuing the traverse. This process can increase the distance a crewmember must travel by as much as three times. Since the travel speed of crewmembers during EVA is deliberately slow, such transfers can be time consuming.

The purpose of the present research is to improve the mobility of tethered EVA crewmembers in micro-gravity. An automated tether management system would simplify tether transfer by allowing a crewmember to remain stationary while remotely opening a tether hook and retracting his or her safety tether. This functionality would be particularly useful in areas of space structures where guide wires may not be present or convenient and during construction of these structures.

Additional potential applications for the automated tether management system include crewmember locomotion and object manipulation. Since the system incorporates a powered tether retractor, a suited crewmember could be safely transported across gaps in a space structure where no handholds are available. With a proper supporting structure, multiple systems could also be used in an antagonistic configuration to manipulate cargo.

The key components of the proposed automated tether system (Figure 2) are a remotely controllable robotic gripper, a power assisted tether retractor, and a hybrid tether that provides tensile support and carries communication signals. The gripper positively engages (fully encircles) an anchor, locks without relying on system power, and is capable of remote disengagement. The retractor emulates existing passive tether retractors (Figure 1b) and adds the capability of active tether retraction. The retractor actively applies a force to the extended tether until the tether and gripper reach a terminal velocity, and then saves power by disengaging the drive mechanism to allow passive retraction. This allows continued tether retraction without consuming power or developing slack. The hybrid tether essentially consists of a Vectran [5] structural weave encasing a single-mode fiber optic core, which transmits commands to the gripper that are entered via a manual interface (not shown) on the retractor.

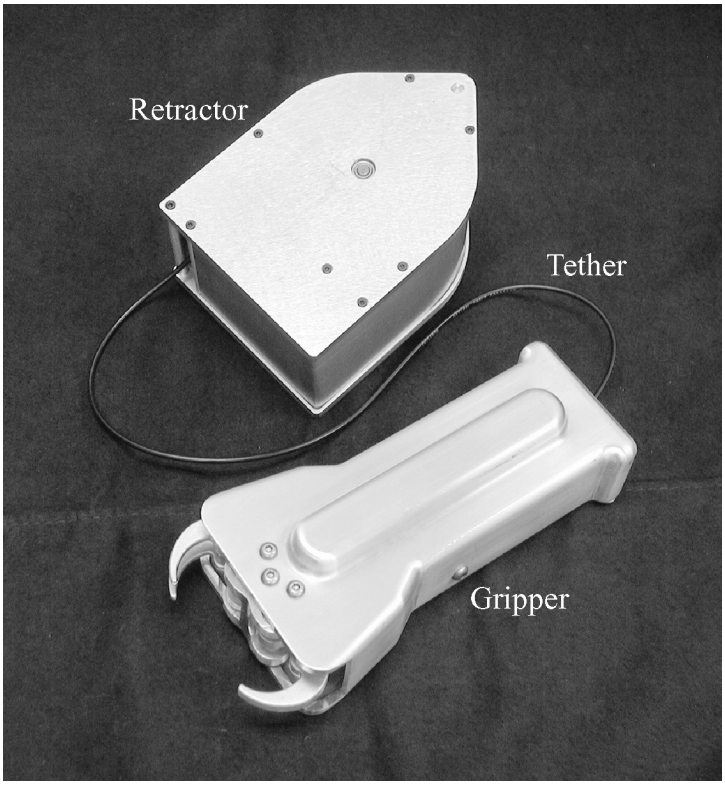

Figure 2. Automated tether management system.

2. BACKGROUND AND DESIGN REQUIREMENTS

The overall goal of the automated tether management system was to meet or exceed the functionality of existing tethering devices in all areas. Most design specifications were established by referencing NASA documents [2-4] that specify requirements for EVA tool performance and describe currently used tools. Additional requirements were then added to provide functionality that surpasses that of existing flight hardware in key areas, such as automation and adaptability in allowable tether anchors. Although independently derived, many of the following gripper requirements coincide with those set by Mahalingam et al. [6] for gripping in space.

Throughout this work, the English system of units (ft-lbf-s) is referenced, as it is the standard used at NASA Johnson Space Center.

2.1. Gripper Specifications

Trade-offs between functionality and size were necessary to yield a suitable gripper design. Multiple degree of freedom (DOF) grippers provide superb functionality and adaptability, e.g., Biagiotti et al. [7], but also require considerable space for packaging actuators and sensors. Passive gripper designs, such as that of Arisumi and Komoriya [8], require minimal space but allow minimal control. The gripper of the present system was required to be an automated, stand-alone, handheld unit, so it was

decided to allow a maximum of one DOF while incorporating as many passive features as viable.

The following requirements were established for the automated gripper in order to meet and exceed the performance of existing tether hooks. Many of these specifications are necessary in order to meet NASA standards for EVA hardware.

2.1.1. Anchor Points

The gripper will be capable of engaging multiple anchor points, which include standard EVA handrails and loops designed for existing tether hooks (see Figure 3), as well as the standard slidewire. This requires the gripper to pass through and securely engage a loop with a 0.75 in minimum inner diameter and thickness of up to 0.5 in, as well as a wire with 0.125 in diameter.

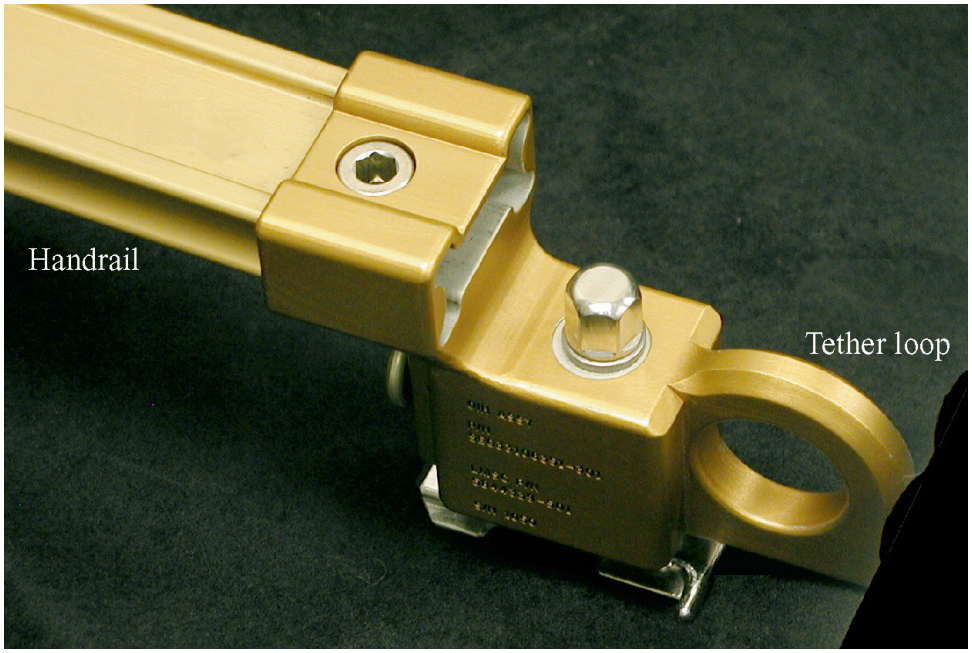

Figure 3. Standard EVA handrail and tether loop.

2.1.2. Gripping

The gripping mechanism will incorporate positive engagement for each anchor with a redundant safety lock. The safety lock will include a clearly visible indication of lock status as well as clear indication of engagement and release procedures. Gripping to each anchor will be versatile, with the ability for either a loose or firm (no-slip) grip. Maximum clamping force will be less than 25 lbf to avoid damage to an anchor.

2.1.3. Loading

The anchored gripper will be capable of supporting an axial load of 400 lbf, which includes a safety factor of 2. The maximum load applied to an EVA handrail will be 300 in-lbf of torsion acting simultaneously with a 50 lbf force in any direction.

2.1.4. Release

The gripper will not release unintentionally. It will allow active remote release as well as manual contingency release. During remote release, there will be minimal force exerted on the anchor by the gripper, keeping the free-floating gripper relatively stationary until it is retracted.

2.1.5. Ergonomics

Manual gripper operation will require less than 30 in-lbf of torque. All forces required from fingers will be between 2 and 10 lbf. The handle of the gripper will have a minimum length of 3.75 in and will incorporate a nonslip, nonabrading surface.

2.1.6. Power Supply

Power will be supplied by an internal battery pack, which will be replaceable at the EVA worksite by a suited crewmember. An indicator will display the level of battery charge.

2.1.7. Degrees of Freedom

The gripper will have one DOF to reduce complexity, save space, and minimize weight.

2.2. Retractor Specifications

The following requirements were established based on existing retractable safety tethers as well as additional features desired of the system.

2.2.1. Loading

The retractor will bring a 550 lb mass at 4 ft/s to a stop with mass attenuation of less than 100 lbf. The minimum design load will be 400 lbf.

2.2.2. Tether Length

The retractor will contain a tether length of at least 50 ft in order to provide functionality similar to existing safety tethers.

2.2.3. Retraction

Retraction will be passive unless a driving force is required. Passive operation will be similar to existing retractable tethers, which require 0.5 lbf to extend the spring-loaded tether and incorporate a friction brake to prevent retraction. The brake is overridden and tether extension accomplished with a 1.5 lbf tether force. The active

drive will automatically engage and disengage the tether reel as required. The maximum retraction rate will be less than 0.5 ft/s, and maximum distance of the gripper from the retractor (which is fastened to the crewmember's chest toolkit) upon return will be 2 ft to ensure that it is within reach.

2.2.4. Power Supply

Power supply requirements are the same as those required of the gripper (see Section 2.1.6).

3. PROTOTYPE SYSTEM DESIGN

3.1. Gripper Prototype

The assembled prototype gripper is shown in Figure 2, with an exploded view shown in Figure 4. The housing serves as a handle for the gripper and provides structural support for the internal mechanism, jaws and tether. A geared motor and a lead screw drive three opposing jaws via parallel coupling linkages. The housing also contains batteries for powering the system and all control electronics. Commands for opening and closing the gripper are received via a fiber optic core at the center of the tether or via tactile switches (not shown) on the handle of the gripper.

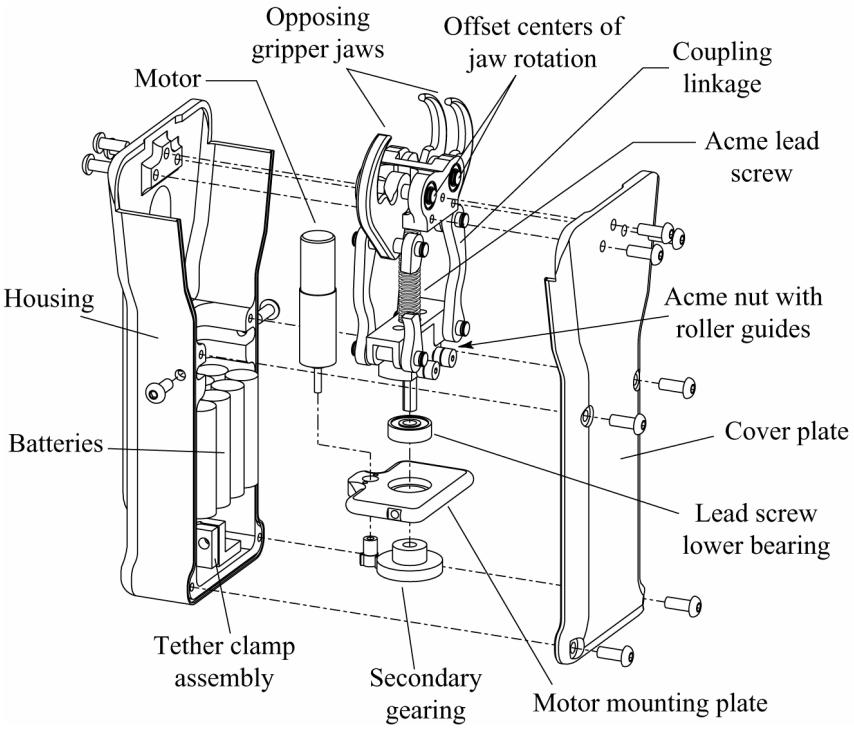

Figure 4. Gripper exploded view.

3.1.1. Jaw Design

A configuration of opposing offset rotating jaws was chosen in order to maintain a single DOF while allowing the jaws to grip objects with large variations in size and shape. The jaws also open widely in a small space, which reduces alignment problems when approaching the object to be gripped (see Figure 5). When closed, the offset jaws intermesh and surround the gripped object in order to achieve positive engagement. The jaws can securely grip an anchor either loosely or firmly by partially or fully closing the jaws, respectively. The purpose of this is to allow, for each anchor, (1) the option of a sliding grip, as might be especially useful on a slide wire; (2) rotation of the gripper and alignment with the tether, as is especially needed when loads are applied to the tether; and (3) the option of a solid grip, which would keep the gripper stationary, even on a slide wire. Inner jaw geometry was designed such that the gripper would engage a variety

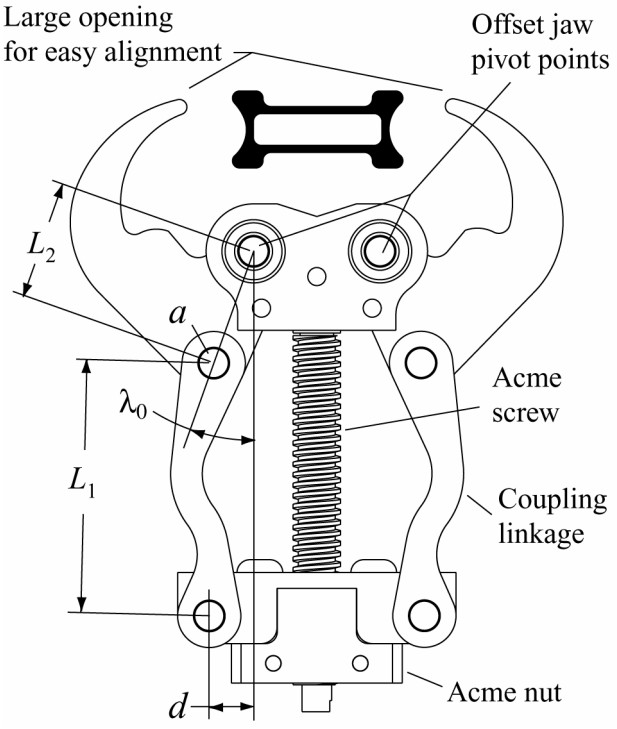

Figure 5. Gripper linkage.

of anchors including the relatively large EVA handrail, standard tether loops, and the small 0.125 in diameter slide wire, which are all shown in Figure 6. Jaw actuation is accomplished by parallel four-bar linkages driven by an acme lead screw (see Figure 4 and Figure 7). Rotation of the acme lead screw causes linear displacement of the acme nut, which in turn causes the coupler links to move and the jaws to rotate. The acme screw is self-locking, allowing the jaws to maintain position without applied power. The gripper thus locks passively and is designed, along with the coupling linkage (described below), to withstand forces at the jaws in excess of 400 lbf.

3.1.2. Coupling Linkage

A four-bar linkage configuration was chosen for its capability to provide relatively constant gripping force on various-sized anchors when properly optimized. The goal of the linkage optimization was to obtain a maximum yet uniform force magnification factor for a variety of anchors while limiting the required travel of the lead screw. This force magnification factor, X_{Fmag}, is defined as the ratio of the maximum force exerted by the jaws, F_{jaw}, on an anchor to the linear force exerted by the acme nut,

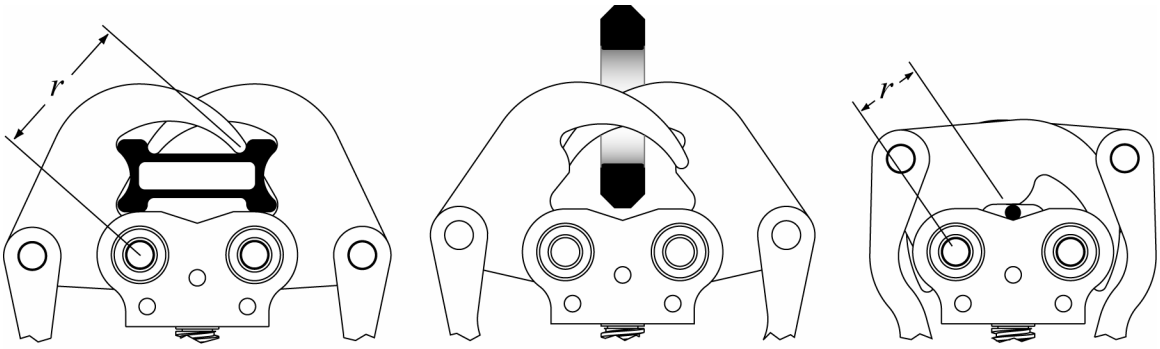

(a) EVA handrail (b) Tether loop (c) Slide wire

Figure 6. Range of gripper applications. The variable effective moment arm, *r*, is shown.

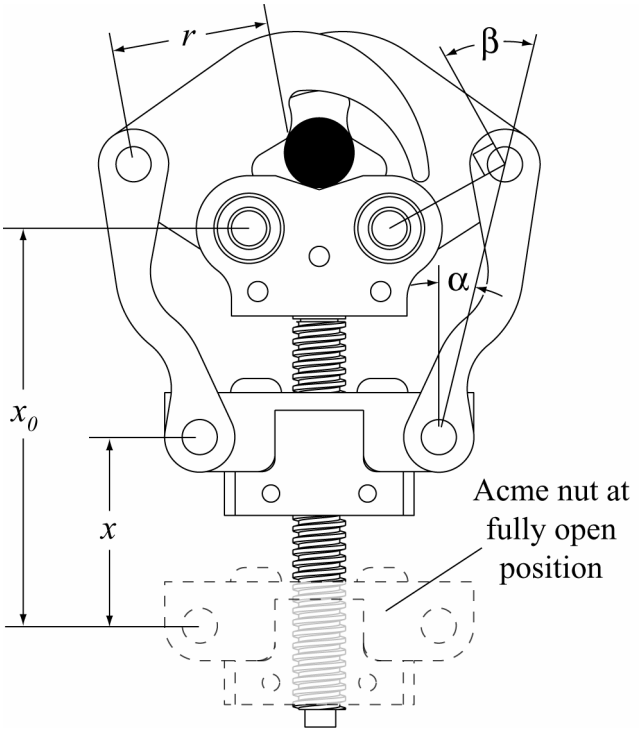

Figure 7. Parameters that determine grip properties.

F_{nut}, or using terms defined in Figure 5 and Figure 7,

$$X_{Fmag} = \frac{F_{jaw}}{F_{nut}} = \frac{L_2}{r}\cos\alpha\cos\beta \tag{1}$$

where

$$\beta = \sin^{-1}\left(\frac{{L_1}^2 + {L_2}^2 - (x_0 - x)^2 - d^2}{2L_1L_2}\right) \tag{2}$$

and

$$\alpha = -\tan^{-1}\left(\frac{d}{x_0 - x}\right) + \sin^{-1}\left(\frac{L_2\cos\beta}{\sqrt{(x_0 - x)^2 + d^2}}\right). \tag{3}$$

The challenge is that the maximum jaw moment arm acting on large objects, such as the EVA handrail (*r*, Figure 6a), is larger than the moment arm acting on small objects, such as the slide cable (*r*, Figure 6c). A constant maximum torque applied to the jaws for gripping all anchors could result in crushing of some anchors and loose gripping of others. Avoiding this was the motivation for selection of four-bar linkages, which were then optimized using constrained gradient-based techniques [9] to find the optimal configuration for gripping several different sized objects. As shown in Figure 5, the parameters varied during the optimization included the horizontal separation, *d*, between the jaw pivot and acme nut pivot, the length L_1 of the coupling link, the length L_2 between the jaw pivot and connection to the coupler link, and the initial angle λ_0 describing the fully-open angular position of the jaw relative to vertical. A composite cost function, *F*, was minimized, which is a 2-norm that includes weighted force magnification factors for four different anchors and the weighted maximum nut travel distance, *D*,

$$F = \left\| \sum_{i=1}^{4} W_i f_i^2 + W_D D^2 \right\| \tag{4}$$

where

$$f_i = 2 - \left(X_{Fmag} \right)_i . \tag{5}$$

In the minimization function, (5) was used for each anchor since the goal was to maximize all values of X_{Fmag} while finding relatively constant values for all anchors. Geometry allowed the possibility of values of X_{Fmag} greater than 1, so in order to assure

maximization, a 2 was used in (5). The factors W_i are weightings for respective elements of the optimization and are described below.

The anchor cross sections included in the optimization were the EVA handrail, a 0.75 in diameter round, a 0.50 in round, and a 0.125 in round. For geometric and packaging purposes, the parameters were constrained such that

$$\begin{gathered} \lambda_{toggle} + 10^\circ \le \lambda_0 \le 180^\circ \\ 0.1 \le L_1 \le 2 \text{ in} \\ 0.94 \le L_2 \le 2 \text{ in} \\ -0.5 \le d \le 0.35 \text{ in} \end{gathered} \tag{6}$$

where λ_{toggle} is the angle describing the toggle position of the linkage. The constraint involving this value prevents the coupling linkage from passing through its toggle point and folding inwardly and provides an acceptable mechanical advantage at the fully open position of the jaws.

Starting the optimization from multiple initial configurations and weightings reliably indicated that the optimum configuration was described by

$$\lambda_0 = 0.29 \text{ rad} \quad L_1 = 2.0 \text{ in} \quad L_2 = 0.94 \text{ in} \quad d = 0.35 \text{ in}$$

which results in a maximum nut travel, D, of 1.73 in and a value of 2.9 in for x_0 (see Figure 7). This configuration is the result of all four optimized parameters lying at the bounds of their respective constraints. The weighting factors W_1-W_4 had no effect on the results of the optimization, but values of W_D between 1 and 0.05 resulted in the length of link L_2 ranging from its lower bound of 0.94 in to 1.35 in. This slightly increased the values of X_{Fmag} for all anchors due to the increased moment arm about the jaw pivot, but

did not appreciably change the relative ratios. This increase in X_{Fmag} came at the cost of an increase in D as well, which ranged from 1.73 in to 2.5 in for the above values of W_D. Minimizing the packaging size of the already relatively large gripper was a high priority, so the weight W_D was kept at a value of 1, which minimized the lengths L_2 and D. Resulting gripping properties for several anchors are summarized in Table 1. The comparison in Figure 8 of X_{Fmag} for these anchors shows that the linkage optimization was successful in obtaining relatively constant values for several anchor sizes.

In Figure 9, angular jaw position is plotted against linear displacement of the lead screw nut for the optimized linkage described above. This plot shows that in addition to achieving a relatively consistent value of X_{Fmag} for each anchor, the linkage provides a roughly linear relationship between the angular motion of the gripper jaws and the linear motion of the lead screw nut. This is beneficial from a controls standpoint, since there are no regions of appreciable jaw acceleration when the motor is moving at a constant speed. The open-loop behavior of the jaws is intuitively predictable by a typical user, with the only significant accelerations of the jaws occurring when actuation is engaged or

Table 1. Gripping characteristics for various anchors.

Anchor	**Moment Arm, *r* (in)**	**Nut Disp., *x* (in)**	**Max Grip Force, F_{jaw} (lbf)**	X_{Fmag}
EVA Handrail	1.27	0.98	16.9	0.676
0.75 in round	1.19	1.26	15.8	0.632
0.5 in round	0.725	1.43	22.6	0.905
0.5 in square	0.728	1.47	21.6	0.865
0.25 in round	0.685	1.62	18.7	0.747
0.125 in round	0.642	1.73	15.3	0.614

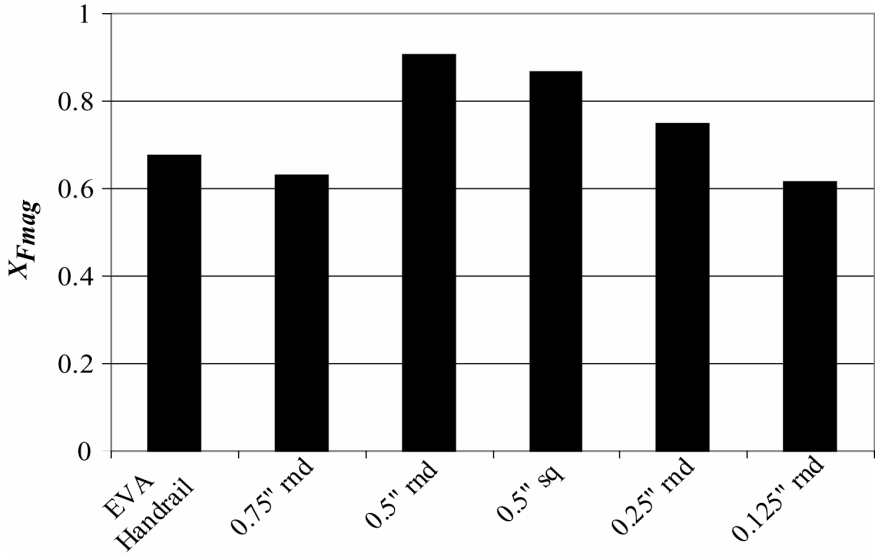

Figure 8. Force magnification factors, X_{Fmag}, for several anchors.

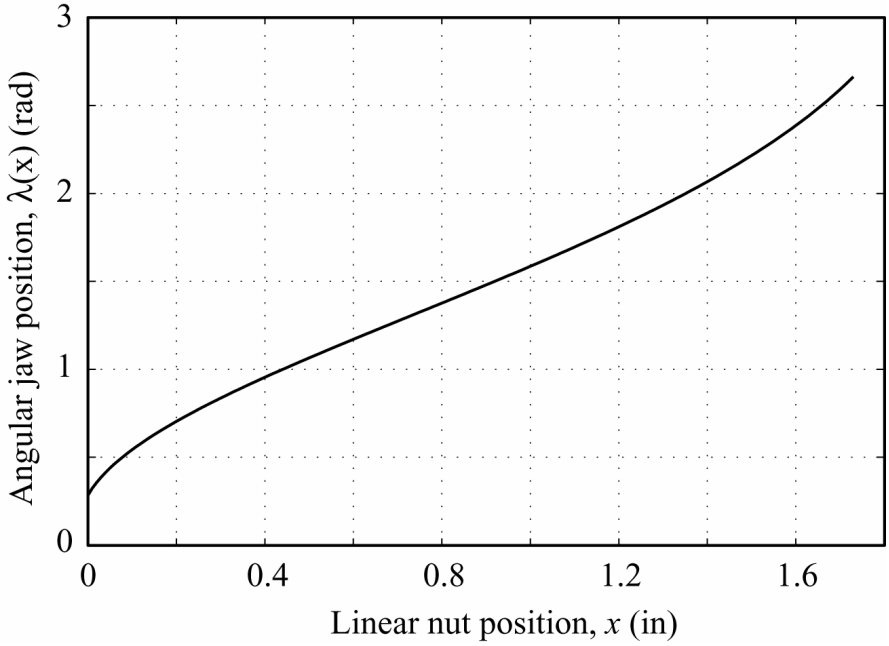

Figure 9. Angular jaw position vs linear acme nut position.

disengaged. If closed-loop control were implemented, no major considerations would be required to account for nonlinear behavior between the nut and the jaws. The influence of various values of the optimization weighting factor W_D on the shape of the curve of Figure 9 was examined to determine their effects. It was found that with values of W_D larger than 1, the curve became less linear, which gives additional motivation for the choice of W_D as 1.

3.1.3. Actuation

Actuation of the gripper is accomplished with a 2.3 watt MicroMo 1528-012BRE brushless DC servo motor with integrated drive electronics, which is suitable for use in a vacuum. It is identical to the motor used in the retractor. The motor is fitted with a 14:1 planetary gearbox (MicroMo 16/7), and drives the 0.375 in, 12 thread-per-in, single-lead acme screw through a 3.75:1 secondary gear stage. Maximum gripping force is approximately 23 pounds on the 0.5 in round, and the designed maximum closing time is approximately 4 s on the 0.125 in round.

3.2. Retractor Prototype

The prototype retractor is shown in Figure 2, with an exploded view in Figure 10. The housing top and bottom plates and midsection contain and provide support to the internal mechanism of the device. A spiral spring and a geared motor provide passive and active retraction actuation, respectively, with a clutch mechanism to switch between modes as required. Commands are sent across the tether from the retractor to the gripper via a fiber optic transmitter coupled to a commutator plate that allows communication

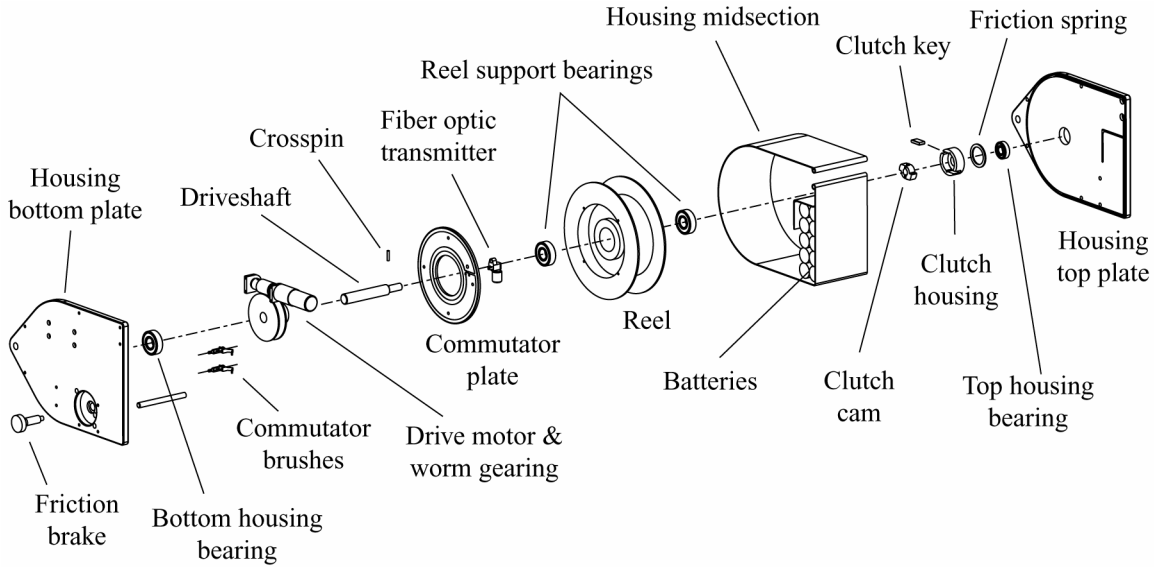

Figure 10. Exploded view of retractor.

between stationary circuitry within the retractor body and the rotating tether on the reel. Batteries and control electronics are also contained within the unit.

3.2.1. Passive Actuation

Spring retraction and a friction brake provide the retractor with passive behavior that is designed to emulate existing retractable safety tethers. A long coil of 0.015 in x 0.125 in spring steel (not shown) provides a relatively constant tether retraction force of approximately 0.5 pounds. Retraction can be prevented by applying a brake, which consists of a spring-loaded friction pad that rubs on the side of the reel. Similar to the retractable safety tether currently in use (see Figure 1b), extension of the tether is still possible once the brake is applied, but a sufficient tether force, adjustable between 0.5 and 2.0 pounds, must overcome the friction.

3.2.2. Active Actuation

The drive motor and worm gearing provide active functionality to the retractor. A MicroMo 1528-012BRE DC brushless motor with a 14:1 planetary gearbox is used,

which is identical to the motor that powers the gripper. A worm gear on the motor shaft mates to a worm wheel that is rigidly coupled to the drive shaft. The drive shaft passes through and supports the reel on its bearings and is in turn supported at its ends by bearings pressed into the housing top and bottom plates. With a single-lead worm stage and 40:1 reduction, active actuation is designed to apply a maximum tether retraction force of 3.8 lbf with a terminal velocity of 0.4 ft/s.

3.2.3. Clutch Mechanism

The clutch mechanism shown exploded in Figure 11 allows switching between modes of passive and active actuation. When engaged, the clutch transmits torque from the motor to the reel. When the clutch is disengaged, the reel is free to rotate bidirectionally relative to the drive shaft via the reel support bearings, allowing it to be driven by the spring.

The clutch housing envelops the clutch cam and provides retaining slots to support the clutch keys as seen in Figure 12a. The clutch cam is rigidly fixed to the

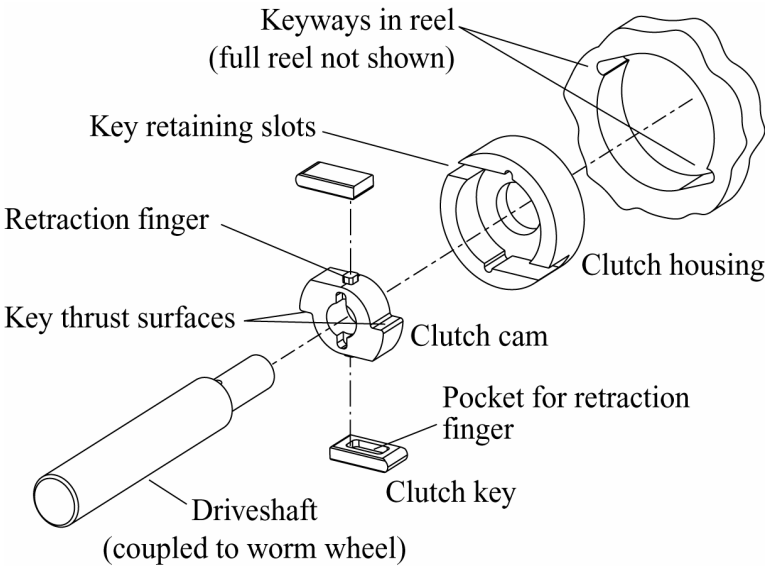

Figure 11. Exploded view of clutch components.

driveshaft, so when the drive shaft rotates, the cam turns relative to the clutch housing, and the thrust surfaces of the cam force the clutch keys outward against the reel (Figure 12b). If the keyways are misaligned (Figure 12c), the clutch housing rotates with the clutch cam until the keyways are aligned with the clutch keys. Once oriented, the clutch keys fully engage the keyways in the reel (Figure 12d), which allows the motor to drive the reel.

The drive system disengages when the motor is deactivated or the spring-loaded reel turns faster than the terminal speed of the motor. This causes the clutch cam to rotate relative to the clutch housing until the fingers engage the key pockets (Figure 13a-c). The clutch cam continues to rotate until the keys are completely disengaged (Figure 13d), and the reel is allowed to rotate independent of the motor. The spring-loaded reel can

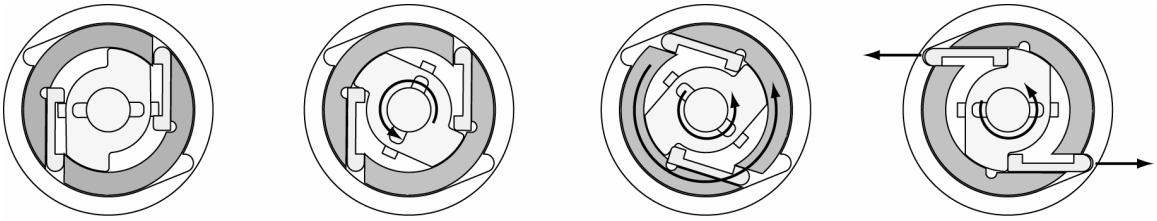

Figure 12. Clutch engagement process.

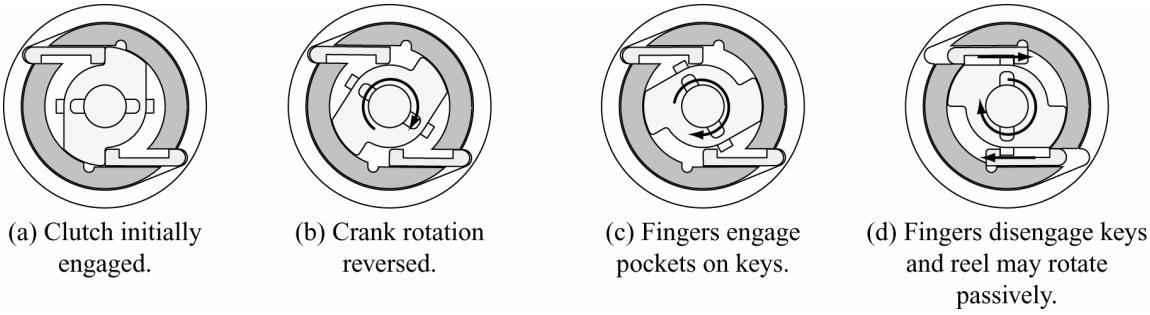

Figure 13. Retractor clutch disengagement.

then passively retract the tether, preventing excess tether from accumulating in the workspace and permitting power consumption to cease.

3.3. Multifunctional Tether and Communications

A sample length of tether was acquired for prototyping that had similar dimensions as that specified for the system, but had differing materials and load capabilities. It is a 0.118 in composite cord that incorporates both tensile structural support and communication transmission. At the core of the tether is a single-mode fiber optic element within a protective plastic jacket. Surrounding this core is an aramid yarn that provides a rated structural strength of 40 lbf and a polyurethane outer coating that contains and provides protection for the aramid fibers and fiber optics [5]. The rated bend radius of this tether is 1.18 in. Although the load limitations of this particular tether preclude its use in a safety tether system, it served as an effective low-cost substitute with properties indicative of the tether of similar construction that was specified for the system.

Commands are transmitted from the retractor to the gripper via the fiber optic element at the core of the tether. This mode of communication was selected because of challenges in the operating environment. Radio communication is not practical due to a lack of available frequencies, infrared transmissions are affected by extreme variations in light levels and blockage of line-of-sight, and long conductors traveling at high velocities through Earth's magnetic field can produce voltages that may damage motors and electronics.

A commutator plate and brushes within the retractor allow an infrared transmitter mounted within the rotating reel to transmit commands from stationary circuitry within

the retractor body. To limit sensitivity to noise, allow multiple command transmission, and prevent false command transmission, a signal encoder/decoder pair is used. The encoder interfaces with tactile switches at the retractor and encodes signals on a 38kHz carrier wave. Commands are transmitted by the infrared emitter through the fiber optic cable to a receiver at the gripper, where they are decoded and executed, allowing remote gripper release and subsequent retraction. The transmitter and receiver are Industrial Fiber Optics, Inc. models IF-E96 and IF-D96, respectively.

4. SYSTEM DYNAMIC MODELS

A dynamic model of the automated tether system was constructed and simulated in order to predict results of testing as well as to investigate orbital effects that cannot be readily tested on earth. An inertial field model was first derived that serves as a basis for more detailed modeling and gives initial indication of retraction dynamics. Translation and rotation of the gripper in two dimensions were modeled in order to provide insight into the dynamics of the current system as well as to verify results of tests to be performed with the system, which were necessarily conducted in a two-dimensional inertial frame (see Section 5 for information on system testing). An orbital model was then developed in order to describe the dynamics that would occur in a system that is in orbit around the earth. Equations of motion were derived using Lagrange's equations [10] with the application of simplifying assumptions as described in the following sections.

4.1. Inertial Field Model

Dynamic equations of motion for spring-assisted retraction of the system in an inertial field served to provide initial insight into the dynamics of the tether system as well as to verify results of retraction tests to be performed on the system. In this derivation, the tether is assumed to be massless and taut at all times, which allows modeling of the coil spring and tether collectively as a massless linear spring and neglects

any dynamics of the tether itself. This is justified under the assumption that the tether has little mass relative to the gripper and exerts negligible forces on the device. Non-conservative forces are assumed negligible since they would result only from friction in the retractor when operated in microgravity.

The system is referenced in the polar coordinate system shown in Figure 14 with the retractor placed at the origin (point O) and the tether attached to the gripper at point A. The kinetic and potential energies for the system are expressed respectively as

$$T = \frac{1}{2} m_g \left(\dot{r}_c^2 + r_c^2 \dot{\theta}^2 \right) + \frac{1}{2} J_g \dot{\phi}^2 \tag{7}$$

$$V = \frac{1}{2} k \left(r_T + r_0 \right)^2 \tag{8}$$

where m_g and J_g are the gripper's mass and rotational inertia about its center of mass, *k* approximates the stiffness of the retractor spring, $r_c = |\overline{r}_c|$ is the distance from the center

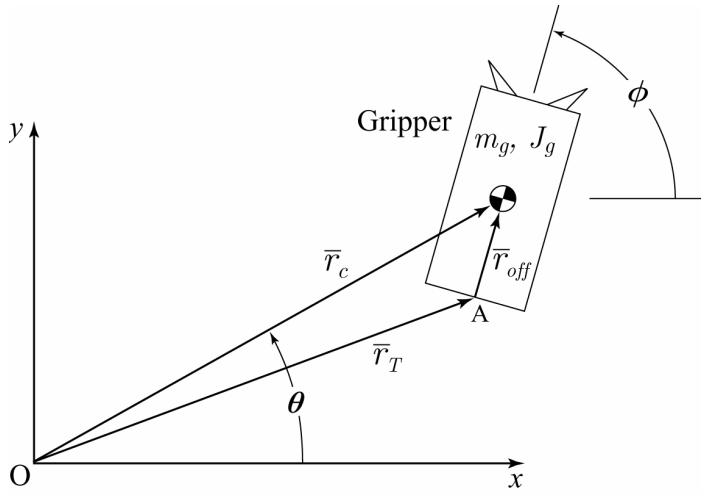

Figure 14. Gripper diagram in an inertial field.

of mass of the gripper to point O, $r_T = \left|\overline{r}_T\right|$ is the length of extended tether, and r_0 provides for the preload of the spring when fully retracted.

The vector $\overline{r}_T$ can be determined by

$$\overline{r}_T = \overline{r}_c - \overline{r}_{off} \tag{9}$$

which allows expression of the potential energy stored in the spring as

$$V = \frac{1}{2}\left(\sqrt{r_c^2 + l^2 - 2r_c l\cos(\phi - \theta)} + r_0\right)^2 \tag{10}$$

where $l = \left|\overline{r}_{off}\right|$ is the offset distance between the attachment point of the tether and the center of mass of the gripper.

With kinetic and potential energies known, the Lagrangian can be calculated by

$$L = T - V\,. \tag{11}$$

With non-conservative forces ignored, the Lagrange equations of motion are then found by

$$\frac{d}{dt}\left(\frac{\partial L}{\partial \dot{q}_i}\right) - \frac{\partial L}{\partial q_i} = 0 \tag{12}$$

where $q = \{r_c, \theta, \phi\}$. The resulting equations of motion are then

$$\ddot{r}_c = r_c\dot{\theta}^2 - \frac{k}{m_g}[r_c - l\cos(\phi-\theta)]\left(1 + \frac{r_0}{\sqrt{r_c^2 + l^2 - 2r_c l\cos(\phi-\theta)}}\right)$$

$$\ddot{\theta} = -\frac{2\dot{r}_c\dot{\theta}}{r_c} + \frac{kl\sin(\phi-\theta)}{m_g r_c}\left(1 + \frac{r_0}{\sqrt{r_c^2 + l^2 - 2r_c l\cos(\phi-\theta)}}\right) \qquad (13)$$

$$\ddot{\phi} = -\frac{kr_c l\sin(\phi-\theta)}{J_g}\left(1 + \frac{r_0}{\sqrt{r_c^2 + l^2 - 2r_c l\cos(\phi-\theta)}}\right).$$

4.2. Orbital Field Model

The purpose of orbital simulations of the system is to explore the dynamic effects of on-orbit retraction of the gripper. The gripper is treated as a particle since it is desired to find the relative translation induced in the gripper due to coriolis effects. The gripper is described in the reference frame of the astronaut, which rotates during orbit in order to maintain a constant orientation relative to the surface of the earth. This orientation of the orbiting frame was chosen since it describes the orientation of the International Space Station, which has the same side facing the earth at all times. The astronaut faces the gripper at the beginning of retraction, but does not rotate to follow the gripper during retraction. The retractor is assumed to be rigidly fixed to the astronaut, and any forces exerted on the relatively massive crewmember due to retraction of the gripper are neglected. The tether and spring are again modeled collectively as a massless linear spring, which requires the tether to be massless and taut at all times. It is also assumed that the crewmember is traveling in a planar, circular orbit, which implies constant velocity and altitude. The altitude of the crewmember's orbit is approximately that of the

International Space Station (~240 mi) with a sustaining speed that balances gravitational and centrifugal forces, or

$$\frac{m_A v_A^2}{r_A} = \frac{m_A \left(\dot{\theta}_A r_A\right)^2}{r_A} = \frac{G m_e m_A}{r_A^2} \tag{14}$$

where m_e and m_A are the masses of the earth and the astronaut, respectively, r_A is the distance from the center of the earth to the astronaut, $\dot{\theta}_A$ is the angular speed of the astronaut's orbit, and v_A is the linear speed of the astronaut.

For calculation of the kinetic and potential energies, the gripper is referenced in the coordinate frame $\hat{e}_1, \hat{e}_2, \hat{e}_3$ shown in Figure 15, where $\hat{e}_1$ remains parallel to $\overline{r}_c$ and $\hat{e}_3 = \hat{e}_1 \times \hat{e}_2$. The position vector of the gripper is then

$$\overline{r}_G = \left(r_c + r_A \cos\gamma\right)\hat{e}_1 - r_A \sin\gamma \hat{e}_2 \tag{15}$$

where r_c and r_A are the respective magnitudes of the vectors $\overline{r}_c$ and $\overline{r}_A$.

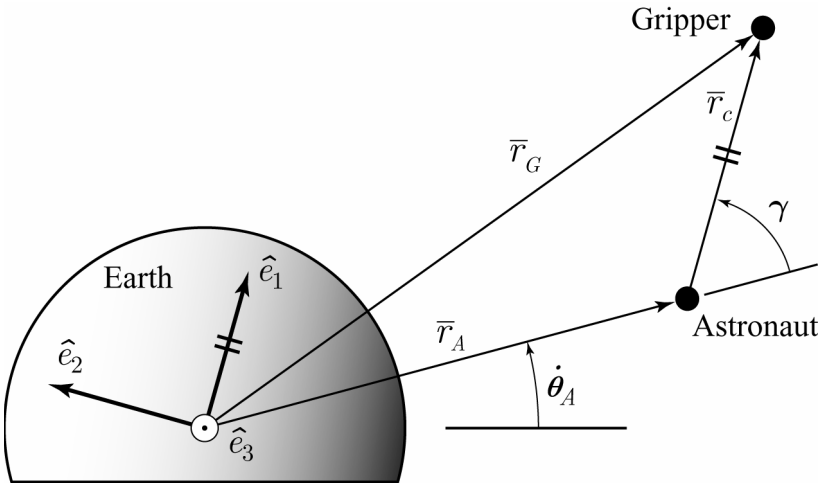

Figure 15. Diagram of system in an orbital frame.

For the sake of simplicity, gravitational potential energy is defined in terms of the acceleration due to gravity at the altitude of the astronaut, which is derived from Newton's law of gravitation,

$$F_g = \frac{Gm_1m_2}{r^2}. \tag{16}$$

Using Equations (14) and (16), the acceleration due to gravity as seen by the astronaut can then be described as

$$g_{eff} = \frac{Gm_e}{r_A^2} = r_A\dot{\theta}_A = 28.55 \text{ ft/s}^2 \tag{17}$$

which is valid under the assumption that the maximum 50 ft difference in altitude between the astronaut and gripper results in a negligible difference in gravitational attraction to the earth.

The expression for kinetic energy of the gripper is then

$$T = \frac{1}{2}m_g\left[\dot{r}_c^2 + r_c\left(\dot{\theta}_A + \dot{\gamma}\right)^2 + 2r_cr_A\dot{\theta}_A\cos\gamma\left(\dot{\theta}_A + \dot{\gamma}\right) + 2r_A\dot{r}_c\dot{\theta}_A\sin\gamma + r_A\dot{\theta}_A^2\right] \tag{18}$$

where m_g is the mass of the gripper. The potential energy is the sum of the potential energy due to the spring and that due to the force of gravity,

$$V = \frac{1}{2}k\left(r_c + r_0\right)^2 + m_gg_{eff}\sqrt{r_c^2 + r_A^2 + 2r_cr_A\cos\gamma} \tag{19}$$

where $\overline{r}_G$ of (15) describes the gripper height for determination of gravitational potential. With the kinetic and potential energies known, the Lagrangian can be calculated from (11).

As described in Section 4.3.1, the results of inertial frame dynamic simulations revealed that even a very weak spring would accelerate the gripper to dangerous velocities, so velocity damping of the retraction was implemented. Although this damping force would in reality be applied to the retractor reel, it is modeled as applied to the gripper for the purpose of simplification. This introduces a nonconservative force into the system, so the form of the Lagrange equation that must be used is

$$\frac{d}{dt}\left(\frac{\partial L}{\partial \dot{q}_i}\right) - \frac{\partial L}{\partial q} = \sum_{j=1}^{N} \overline{F}_{nc,j} \bullet \frac{\partial \overline{r}_j}{\partial q_i} \tag{20}$$

where $q = \{r_c, \gamma\}$. The only nonconservative force in the system is that due to damping,

$$\overline{F}_{nc} = -B\dot{r}_c\hat{e}_1 \tag{21}$$

where B is a damping coefficient. The vector $\overline{r}_j$ in (20) that describes the point of application of this force is simply the position vector of the gripper relative to the astronaut,

$$\overline{r}_j = \overline{r}_c = r_c\hat{e}_1. \tag{22}$$

The final equations of motion for the orbital model are

$$\begin{aligned} \ddot{r}_c &= r_c\left(\dot{\theta}_A + \dot{\gamma}\right)^2 + g_{eff}\left(\cos\gamma - \frac{r_c + r_A\cos\gamma}{\sqrt{r_c^2 + r_A^2 + 2r_c r_A\cos\gamma}}\right) - \frac{k}{m_g}\left(r_c + r_0\right) - \frac{B}{m_g}\dot{r}_c \\ \ddot{\gamma} &= -\frac{2\dot{r}_c}{r_c}\left(\dot{\theta}_A + \dot{\gamma}\right) - \frac{g_{eff}\sin\gamma}{r_c}\left(1 - \frac{r_A}{\sqrt{r_c^2 + r_A^2 + 2r_c r_A\cos\gamma}}\right). \end{aligned} \tag{23}$$

4.3. Simulation Results and Discussion

4.3.1. Inertial Field Model

Simulations run with the inertial field model immediately indicated that pure spring retraction is not feasible due to the large speeds induced by the continuous force applied to the free-floating gripper. According to these simulations, if the 0.015 in thick spring were used that provides the design force of relatively constant 0.5 lbf, the gripper would be accelerated to a speed of 22 ft/s when retracted from a distance of 50 ft. Even with a much smaller spring of thickness 0.007 in, which provides roughly 1/10 the force of the 0.015 in spring, the gripper would be accelerated to a speed of 7.6 ft/s. It is therefore clear that simple spring retraction is not a satisfactory method of gripper retraction. One solution to this problem is the inclusion of velocity damping to the retractor reel to prevent retraction speeds from becoming large. This addition of damping was explored in the orbital model and results are described below in Section 4.3.2.

Although pure spring retraction was found to be much too strong for safety, the results from the inertial-field model provide insight regarding the dynamics inherent to the system. Figure 16 shows the path of the gripper as well as schematics of its position and orientation at regular intervals during three cases of retraction with the smaller 0.007 in spring. It is shown that with angular misalignments of $\pi/4$ rad, the gripper undergoes multiple, increasing angular oscillations that grow as large as 1.5 rad with angular velocities as high as 2.7 rad/s. These effects are due to the offset between the gripper's center of mass and tether attachment point. The oscillations of the gripper are likely to be strongly influenced by properties of the tether and are apt to induce waves in the tether. This indicates that neglect of tether dynamics introduces a large amount of error into the

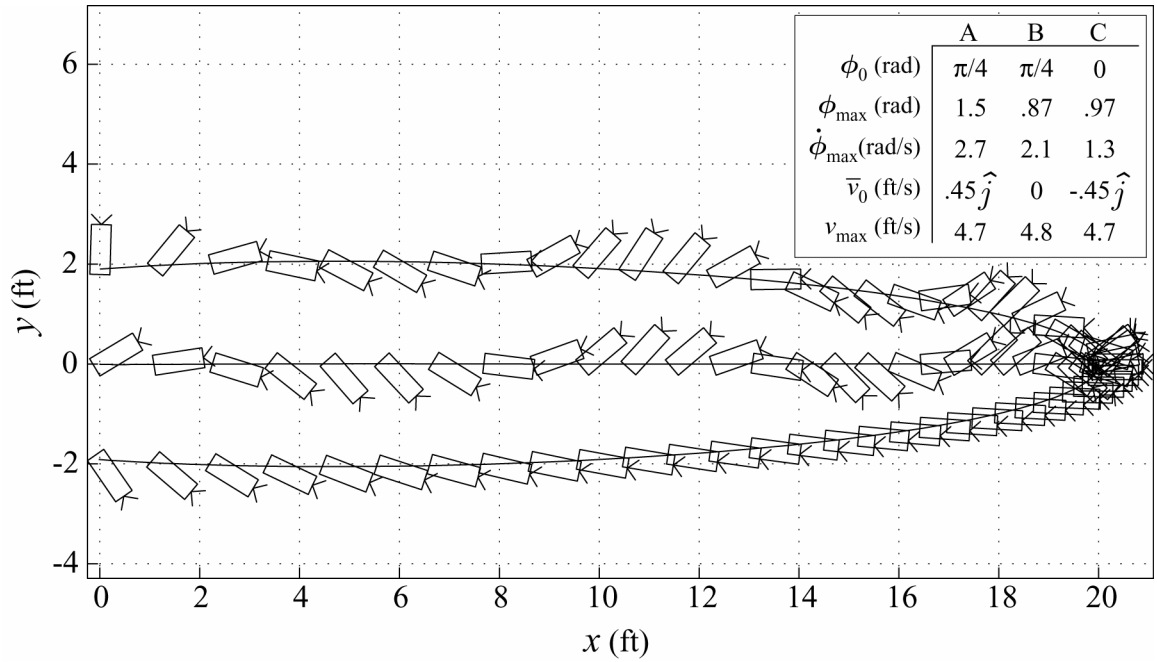

Figure 16. Simulation results with 0.007 in spring in an inertial reference frame with various initial conditions.

system model. The length of tether was restricted to 20 ft in this simulation because with an initial lateral speed of 0.45 ft/s (cases A and C), the drift of the gripper upon arriving at the *y* axis was within the 2 ft limit defined in Section 2.2.3. The speed limit of 0.5 ft/s is, however, violated by speeds of approximately 4.7 ft/s, and will be addressed in the following section as results of velocity damping are introduced.

4.3.2. Orbital Model

The results of the orbital simulations are transformed to the reference frame of the astronaut, $\hat{e}_{1,A}, \hat{e}_{2,A}$, shown in Figure 17. The astronaut faces in the direction of the vector $\hat{e}_{1,A}$, which is described by the initial angle γ_0, throughout the retraction of the gripper. This means that the astronaut faces the gripper at the beginning of retraction and does not rotate to follow it as it retracts. The transformations

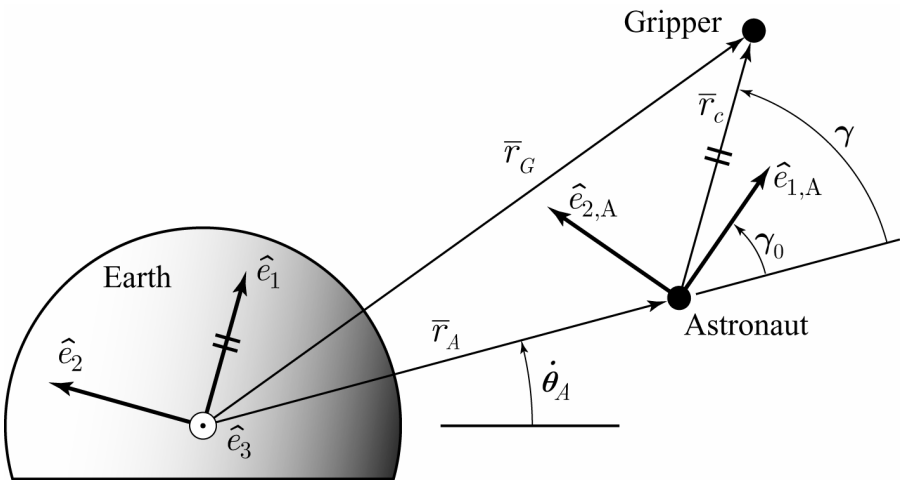

Figure 17. Orbital model including astronaut's reference frame.

$$\begin{aligned} r_{1,A} &= r_c \cos(\gamma - \gamma_0) \\ r_{2,A} &= r_c \sin(\gamma - \gamma_0) \end{aligned} \tag{24}$$

are used to place the gripper in a cartesian reference frame relative to the astronaut.

Simulations of the system in orbit showed that coriolis acceleration significantly influenced the behavior of the gripper during retraction. Figure 18 shows results of retraction of the gripper from a distance of 50 ft along the $\hat{e}_{1,A}$ axis with a 0.007 in spring and sufficient damping to keep the gripper within the 0.5 ft/s speed limit when it reaches the astronaut. While this damping keeps the gripper within safe speed limits, retraction from this distance allows coriolis effects to cause the gripper to drift laterally until it is more than 6 ft from the astronaut when it reaches the $\hat{e}_{2,A}$ axis. It should be noted that the slowing of the gripper shown in this figure is due to modeling error and is addressed below.

The retraction characteristics shown in Figure 18 indicate that retraction of the gripper from a distance of 50 ft is not possible without violating either the speed or drift

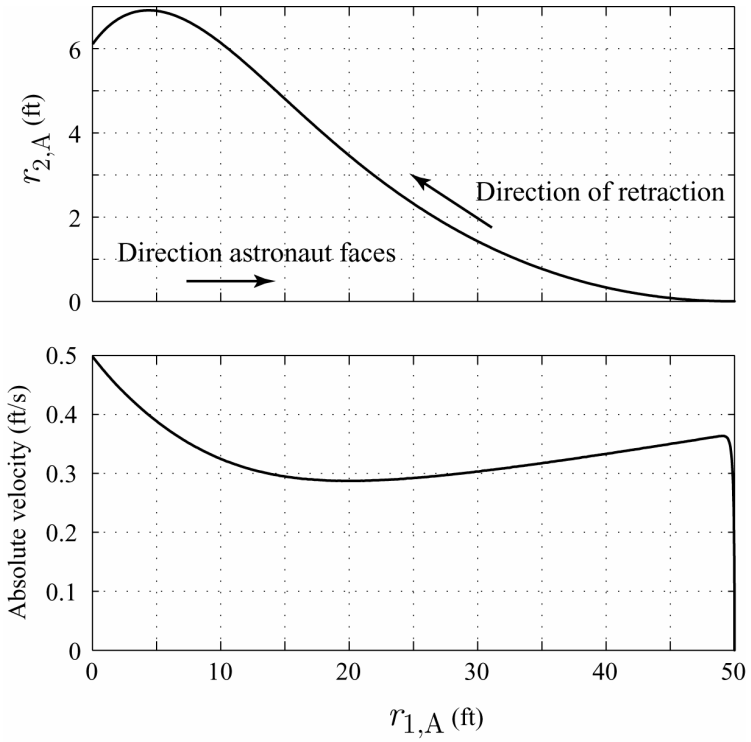

Figure 18. Coriolis effects on gripper position and velocity when retracted with damped 0.007 in spring.

constraints set forth in Section 2.2.3. The amount of drift shown in Figure 18 can be rectified by decreasing velocity damping, but the gripper would return to the astronaut at a speed that violates the safety constraint of 0.5 ft/s. These results indicate that there exists a maximum distance from which the gripper can be safely retracted for given spring or damping characteristics. Figure 19 shows the simulated paths and velocities of the gripper when retracted from maximum allowable distances for both the 0.015 in and 0.007 in springs. In both cases, the lateral drift upon return is 2 ft and the maximum speed reached by the gripper is 0.5 ft/s. Under these constraints, the maximum safe retraction distance was found to be 25.9 ft and 28.5 ft for the larger and smaller springs, respectively. The times required to retract the gripper from these distances were 76.9 s and 85.1 s, respectively. These plots show that the combined effects of the spring and

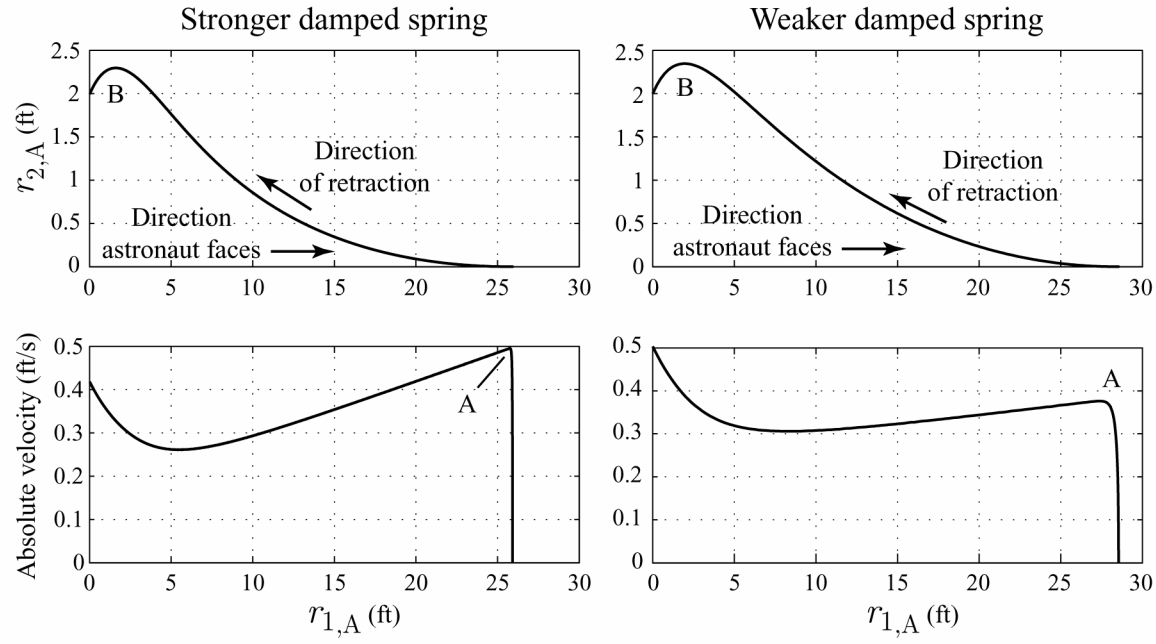

Figure 19. Optimal retraction trajectories and speeds for 0.015 in spring and 0.007 in spring.

damping cause the gripper velocity to quickly increase to a peak value (points A), and then decrease until it approaches the astronaut, where it increases once more due to its being pulled in from its deviating path by the taut tether. The trajectory plots show that the gripper drifts away from the $\hat{e}_{1,A}$ axis on which the tether was initially aligned, then as it approaches the astronaut, the retraction force vector from the taut tether approaches a direction that is normal to the path, and it is accelerated towards the crewmember.

This gripper velocity response indicates significant errors introduced by the simplifications that were applied to the model of the system. Since the derived equations describe the motion of the gripper, a damping force can be applied only to the gripper rather than to the retractor reel. The gripper's velocity could not appreciably decrease in microgravity unless the tether was stiff enough to withstand significant compressive forces without buckling. After reaching the initial peak in velocity (points A), the gripper

will in reality continue at this speed while the retraction of the tether slows under the influence of the damped, decreasing spring force applied to the reel, which results in a loose tether. In addition, the acceleration occurring in the simulation as retraction finishes is due to a taut tether accelerating the deviating gripper towards the astronaut. If the tether became loose as described above, the assumption of a taut tether would be violated and this acceleration would not occur, resulting in additional drift of the gripper upon reaching the $\hat{e}_{2,A}$ axis and a possible continuation of decelerating tether retraction. It is again evident that tether properties must be included in modeling in order to produce results that give a clear picture of the dynamic characteristics of the system.

The retraction behavior of the gripper was found to be independent of the value of γ_0. Each orbital simulation scenario described was run with γ_0 varying between 0º and 360º at 1º increments. Upon comparing the results of these 360 simulations for each scenario, the maximum difference of any one point in the $r_{1,A}$ vs $r_{2,A}$ plot was found to be less than 1.25 in, which can be attributed to numerical simulation error. This result is interesting in that the gripper will behave the same from the veiwpoint of the astronaut (within the orbital plane), no matter what direction the astronaut faces.

4.3.3. General Discussion of Simulation Results

Simulation results showed that spring retraction, as designed, brings the gripper to dangerous speeds when retracted over any appreciable distance. With a relatively constant force of this magnitude applied to the gripper, it continuously accelerates over the entire distance of retraction. Velocity damping restricts this force when undesirable speeds are reached, but as the orbital simulations showed, the effect of a spring force that decreases as the tether retracts together with a constant damping coefficient result in

deceleration of the reel after the initial peak velocity is reached. Since the gripper cannot be slowed by the tether, it will overtake the tether and may return to the astronaut while the tether continues to retract. This is likely to cause additional lateral offset as the gripper returns. Since the tether is not taut as the gripper approaches the astronaut, it cannot cause the path correcting acceleration toward the astronaut that is seen in Figure 19 at points B.

A solution to this problem would be a truly constant-force spring or a spring that applies a slowly increasing force as the tether is retracted. A damped, constant-force spring would keep tether retraction at a constant maximum speed and prevent loose tether from accumulating as the gripper travels to the astronaut. A damped increasing-force spring would likely be more desirable. In this case, the gripper would be quickly brought to a certain speed, and then continually accelerated at a very slow rate, keeping it under a degree of control of the slightly taut tether. Figure 20 shows the retraction characteristics of both a damped constant-force spring and a damped increasing-force spring. The constant-force scenario requires the least time of the two since the gripper travels at a higher speed for a longer period of time, but the validity of the assumption of a taut tether is less sure since there is less acceleration after the initial peak. There is some acceleration of the gripper due to its deviation from the $\hat{e}_{1,A}$ axis, which may provide sufficient control, but a more detailed model that includes tether properties is needed in order to find an optimal retraction profile. Of the options explored thus far, the damped increasing-force spring scenario is the preferred method of retraction. Tension is maintained in the tether throughout retraction, which provides the maximum amount of control possible when using a single extended cable. The maximum allowable retraction

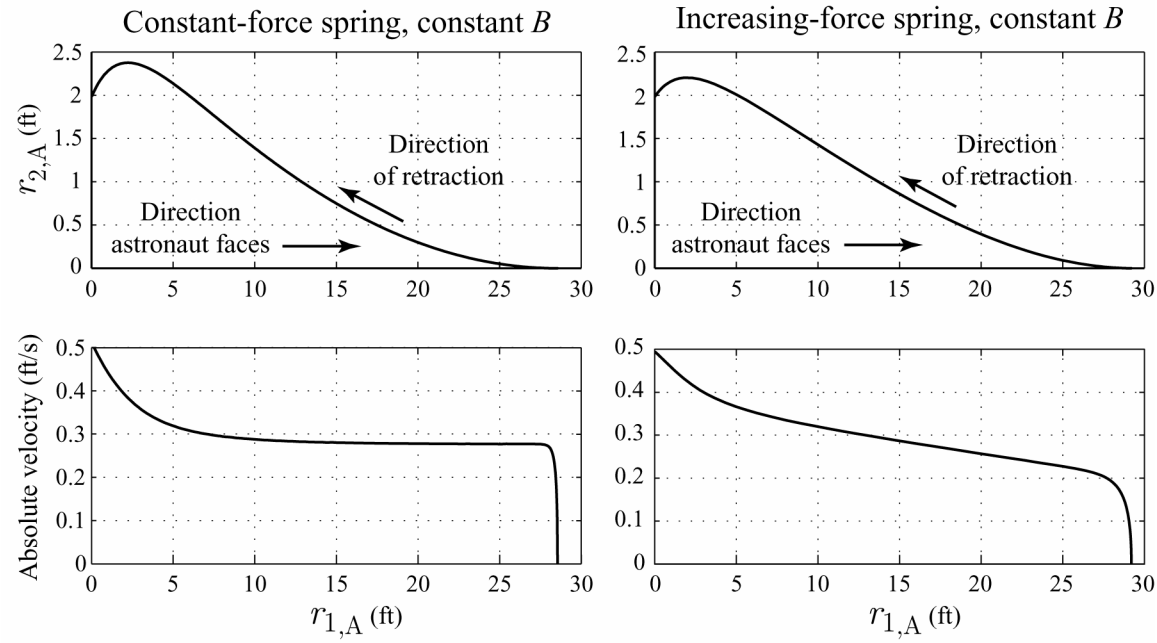

Figure 20. Hypothetical retraction profiles.

distance is also the greatest of all current options, as shown in Figure 20, which shows a maximum distance approaching 30 ft for the damped increasing-force retractor spring.

Tether characteristics were found to be important in describing the dynamics of the system during retraction. The inertial frame results showed that when the gripper is not aligned with the tether when released, multiple angular oscillations result, which would cause significant interaction between the gripper and the tether. In the case of the orbital simulations with simple coil springs, tension in the tether was not maintained, and the gripper overtook the tether as the retractor reel slowed. In order to more fully understand the dynamics of the gripper when retracted, properties of the tether must be taken into account. The tether that was chosen for the current system is a multilayered composite with highly complex static and dynamic properties, and modeling of this magnitude is beyond the scope of the current research.

Coriolis acceleration was found to have significant impact on the behavior of the gripper during in-orbit retraction. This acceleration caused lateral drifting of the gripper relative to the viewpoint of the astronaut that is unacceptable when retracted from a distance of 50 ft. It was therefore determined that use of the automated tether system on orbit would require restriction of the maximum tether length to be somewhat less than 50 ft. The actual maximum allowable tether length cannot be determined with the present model due to the error introduced by simplifying assumptions. Aside from causing lateral offset of the gripper upon return to the astronaut, coriolis acceleration also introduces the possible danger of unexpected collisions of the gripper with other objects as it retracts. Rebounding of the gripper after a collision is highly random and would produce largely unpredictable dynamics.

Finally, it should be noted that these simulations assume no disturbances seen by the gripper during retraction. Since the gripper can be controlled only with tensile force from the tether, a collision or other disturbance that applies forces in any direction other than against the tether cannot be counteracted and would have significant influence on the dynamics of the gripper. A margin of safety that reduces the maximum length of tether will likely be needed to allow for disturbances in order to be statistically confident that the gripper will travel at safe speeds and be within reach of the astronaut upon return.

5. SYSTEM TESTING

Experimentation with the automated tether system was important in order to verify design specifications and reveal potential problems in the system that were not foreseen during design. Capabilities of both the retractor and gripper were measured and compared to designed specifications. The fully assembled system was also tested using an air bearing facility, which served as a simulation of microgravity in two dimensions.

5.1. Experiment Design

Experiments were designed to provide key information about each component of the tether system in order to evaluate system capabilities. Digital video was the primary form of acquired data due to its high data density and relative ease of capture. Visual displays relayed information to the video from sensors measuring values such as voltage, current and tether force. Tether forces were measured with a 25 lbf capacity FUTEK tensile/compressive force sensor. Tether length measurements were taken by placing visible marks on the 45 ft tether at 3 in increments and later taking measurements via video analysis.

5.1.1. Gripper Test Design

The initial tests performed on the gripper were of qualitative functionality. These tests included grasping ability with the main anchors targeted for the device, namely the standard tether loop and EVA handrail. The gripper was tested with each of these

anchors to define the maximum allowable misalignment for a successful grip as well as the amount of gripper movement that a loose grip would permit.

Tests of controls of the gripper mainly entailed measurements of open and close time and amount of overshoot. The gripper cover plate was removed to expose the inner mechanism and give more visual reference for video analysis. Since no loads were applied to the jaws, the remaining housing provided sufficient support to the jaws and inner mechanism, which avoided significant alteration in performance. The jaws were fully closed and opened several times at various motor voltage levels while recording with video to measure the open and close times and amount of overshoot after motor deactivation.

An air bearing table was used to conduct further gripper tests designed to help determine the dynamics induced by release from an anchor in microgravity. The virtually friction-free surface of the air bearing table simulated this environment in two dimensions. The table was a 4 ft x 8 ft x ~1.5 ft slab of granite machined to an ultra-flat surface and leveled to within a slope of $2x10^{-5}$, which created a nominal 20 μg environment. Levitation was achieved with an 8 in diameter air bearing (see Figure 21a) that consisted of aluminum honeycomb sandwiched by two circular, highly smooth glass plates [11]. A single orifice in the center of the bottom plate provided a maximum of approximately 0.0002 to 0.0004 in of levitation by expelling gas that was stored in a lightweight onboard aerosol canister. A flow control nozzle allowed approximately 3 minutes of useful levitation after filling the canister with gaseous difluoroethane (Dust-Off®, [12]) to a pressure of approximately 72 lbf/in^2. In order to minimize unwanted disturbances during testing, a phototransistor circuit that was controlled with direct

incandescent light was used to activate and deactivate the gripper. Figure 21b shows the gripper on the air bearing together with the gas reservoir and required control electronics. A similar air bearing facility setup was used for initial prototype testing of a free-flying inspection robot for space, AERCam [13], which is currently under development by NASA.

In order to study the amount of translation and rotation induced by release, the gripper was secured to the tether loop and the handrail in three orthogonal orientations. The gripper was then opened and released several times from each anchor in each orientation and the resulting behavior was recorded via video.

5.1.2. Retractor Test Design

The initial tests performed for characterizing the retractor were of general suitability, such as winding characteristics and capacity of tether containment. Since the retractor lacks a method of guiding the tether onto the reel, it was important to determine the need for such a feature. Also, the retractor reel was initially designed to contain a

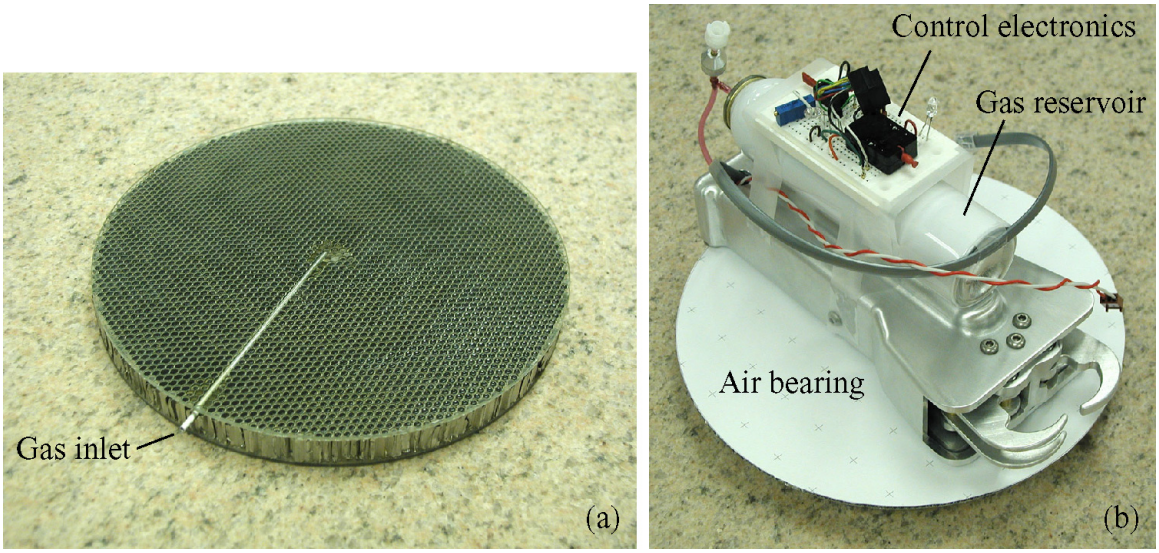

Figure 21. Air bearing equipment for gripper testing.

tether length of 50 ft, so this ability was tested. The tether was fully extended and then retracted using the motor drive with varying amounts of resistive tension. For each test, when the wound tether on the reel began binding against the retractor housing (taken to signify the maximum capacity of the reel), the length of retracted tether was recorded. Throughout all retractor tests, the reel was observed in order to qualitatively determine the winding density. This was possible by using the partial housing midsection shown on the retractor in Figure 22, which allowed observation of the reel without affecting winding performance.

Retraction force profiles for both the spring and motor were obtained using information from the FUTEK force sensor as shown in Figure 22. The sensor was secured at each end with pin joints to avoid unwanted torques. The retractor and sensor both rested on a bearing material consisting of a mixture of miniature plastic balls (diameter ≈ 0.024 - 0.037 in) and cornmeal [14] to minimize force contributions of static

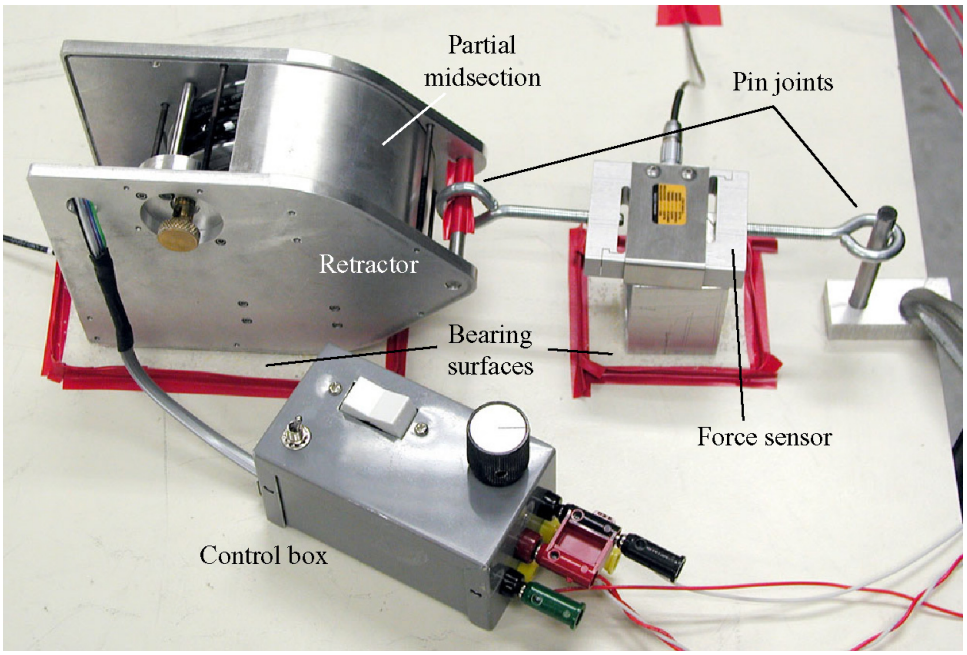

Figure 22. Experimental setup for force capabilities of retractor.

friction. The tether was fully extended, then retracted and stalled at each of the 3 in tether marks until the filtered force sensor reading settled. Although the motor of the retractor would not likely be stalled when used as an active safety tether, stall forces are readily measurable and provide information about maximum motor capabilities. Also, if the system were used for antagonistic parallel wire manipulation, motor stalling data would be important for defining system behavior and capabilities.

Retraction speed capabilities of the retractor motor were measured at several motor voltage levels by fully extending the tether and video-recording retraction until initial binding of the tether on the retractor housing was observed. The markings on the tether combined with timing information on video allowed generation of a retraction speed profile. During retraction, the tether was guided by hand at a distance of approximately 3 ft from the retractor in order to align it with the retractor and introduce as little force on the tether as possible.

5.1.3. Full System Retraction Tests

In order to better understand retraction dynamics of the full tether system, and to verify simulation results, retraction performance was tested on the air bearing table used for gripper testing. The system was fully assembled and the gripper was secured to an anchor while being levitated by the air bearing. The gripper was then opened and retracted approximately 27 in by the retractor under both active and passive modes. Tests were performed with and without initial tension applied by the retractor, and at various angles of alignment between the gripper and the tether.

5.1.4. Communications Testing

In order to focus experimental efforts on the mechanical aspects of this system, testing of communications between the retractor and gripper was not conducted. Fiber optic communication is widely used in industry and it was taken for granted that a system could be developed that would be appropriate for the automated tether system. Primary electrical components were selected and required space was reserved within each device, but actual implementation of the communication function was forgone.

5.2. Experimental Results and Discussion

5.2.1. Gripper Results

The gripper interfaces well with the targeted anchors. The jaws mate well with the shape of the handrail, providing an extremely firm grip, and as long as the jaw tips reach past the far side of the handrail without interference, the jaws automatically align the gripper for a proper grip when closing. Similarly, the only mechanical requirement for a suitable grip on the tether loop is that the jaw tips pass through the center of the loop. A loose grip on the handrail is fairly restrictive but a loose grip on the tether loop is very flexible when the jaws are oriented as shown in Figure 6b. The maximum range of angular movement with a loose grip is 26º on the handrail and 162º on the tether loop. At full motor voltage of 12 V, minimum close time was 2.8 s for the handrail, 3.3 s for the tether loop, and 5 s for full closure, which is acceptably close to the original design goal of 4 s for full closure.

Since there is currently no feedback control implemented for the gripper, the amount of overshoot seen after cutting motor power was measured. When operating at steady state speed at the full motor voltage of 12 V, the significant amount of rotational

inertia inherent to the geared motor, lead screw, and secondary gearing caused the lead screw nut to continue traveling an average of 0.088 in after cutting power, as seen in Figure 23, where the time of 0 s represents the instant of turning off the motor power. On average, the nut settled to within 95% of this value in 0.427 s. Figure 23 shows the average response of 16 test runs of both opening and closing the gripper at full power, bracketed by the 95% confidence intervals of the raw data. Due to the characteristics of the four-bar linkages described by Equations (2) and (3), the maximum angular overshoot of the jaws occurs at the fully open and closed positions, with respective values of 14° and 12°. Although these are the maximum values at the limits of the lead screw motion, typical values of overshoot over the majority of the jaws' range of motion were between 5° and 8°.

Using the air bearing facilities, the dynamics induced by release of the gripper

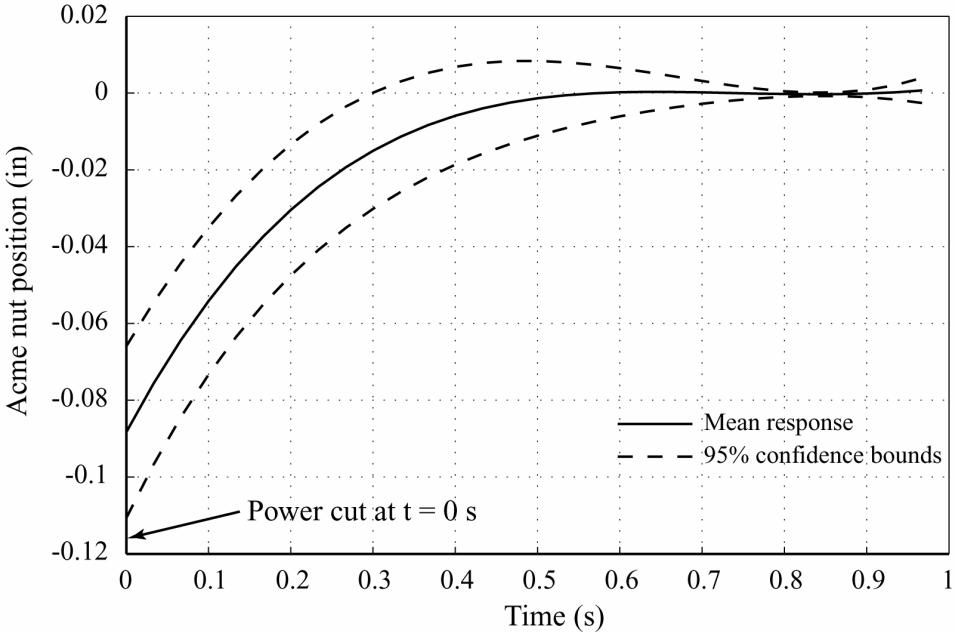

Figure 23. Overshoot of gripper lead screw nut at full motor power (12V).

from an anchor were recorded in three orthogonal planes. Small amounts of translation and rotation resulting from the dynamics of the gripper's internal mechanism were measured when it was released alone from an anchor. As described in the following section, it was found that these small dynamics were insignificant in relation to other effects, such as tether forces, and were thus not analyzed in detail.

5.2.2. Discussion of Gripper Results

Interfacing of the gripper with the tested anchors met and exceeded expectations. The main result obtained was that the EVA handrail is much better suited for a tight grip while the tether loop is best suited for a loose grip. As shown in Figure 6a, the gripper jaws interface closely with the outer contour of the EVA handrail, providing a very solid engagement. When loosely interfacing with a tether loop, as shown in Figure 6b, large amounts of rotation are possible, which allows alignment of the gripper with the tether even when the tether is oriented parallel to the supporting surface of the tether loop. The result is a reduction in the possibility of unacceptable moments applied to the tether loop. The lead screw is a successful locking mechanism that fully prevents backdriving of the jaws and contributes to the strength of grip possible on the handrail.

Some drawbacks inherent to the gripping properties of the gripper have been identified. When gripping the handrail firmly, large moments can be introduced to the handrail due to the long, solid body. Although the gripper is capable of a loose grip on the handrail, the range of possible orientations is very limited, which in turn limits the amount that moments introduced to the handrail can be reduced by aligning the gripper with the tether. In addition, due to the square cross-section of the tether loop, as the jaws

close into a firm grip on this anchor, the gripper is forced into a skewed position, making a firm grip on the tether loop less desirable.

Although tests were carried out to measure translation and rotation of the gripper induced solely by its internal mechanism during release from an anchor, later retraction tests with the full system revealed that the static and dynamic forces of the tether were so much more influential in the behavior of the gripper during release and retraction as to make these small internal dynamic forces insignificant (see Section 5.2.5).

Results from overshoot tests of the gripper showed open-loop control to be suitable for this device. The amount that the jaws overshoot after cutting power is relatively small, and highly accurate positioning of the jaws is not necessary for a satisfactory grip, either loose or firm. The overshoot response is most sensitive at the fully open and fully closed positions, but at these positions, the likelihood that accurate positioning would be needed is remote.

5.2.3. Retractor Results

Tether winding behavior of the retractor was very good considering the lack of a guide mechanism. The tether naturally tended to compactly fill the width and depth of the reel, resulting in generally dense winds, as seen in Figure 24, which shows the result of retracting the tether with a small amount of tension applied to the tether. The average tether length capacity of the reel was 31.5 ft, and ranged from 26 to 36 ft, which is well short of the 50 ft design goal. The capacity of the reel was not significantly affected by the amount of tension on the tether during retraction. Tests conducted with tether tension of less than 0.1 lbf showed winding results that were very similar to tests where frequent

Figure 24. Typical tether wind on retractor reel.

tether tension was sufficient to stall the motor at full power, giving about 1 - 1.75 lbf of force.

Retraction force profiles for both the spring and motor over the retractable length of tether are shown in Figure 25, which shows the tether force required to stall retraction at 1 ft increments. Two curves for the motor stall force reflect the fact that this force peaked immediately after the tether motion was stopped, and then settled to a lower steady value, as described below. As expected, all results show a force gradient that generally decreases as more tether length is taken onto the reel. This is due to the increasing equivalent radius of the reel. The resulting increase in the effective moment arm of the reel decreases the force that is exerted on the tether by the relatively constant torque sources.

Figure 26 shows the speed characteristics of the retractor with a minimal force (under 0.1 lbf) applied to the tether. These profiles show an expected increase in speed as

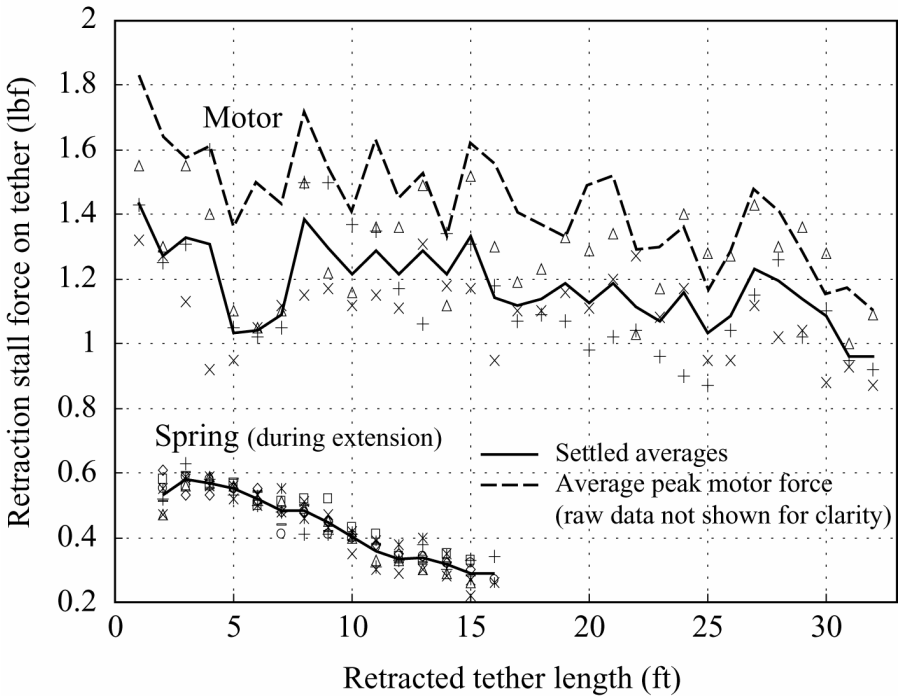

Figure 25. Stalled retraction force profiles for motor and spring.

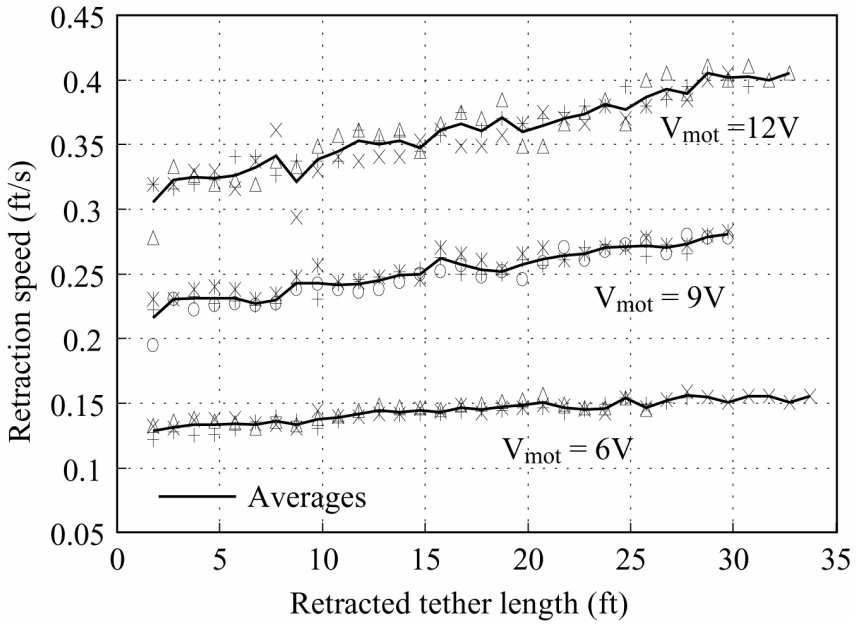

Figure 26. Minimal-load motor retraction speed.

the amount of retracted tether increases. As tether accumulates on the constant-speed reel, the resulting increase in effective reel radius causes the tether retraction speed to increase. The profiles show that at full motor voltage (V_{mot} = 12V), the tether reaches a speed of approximately 0.4 ft/s for the amount of tether that would fit on the reel. By extrapolating this trend, a maximum speed of 0.46 ft/s is indicated for a retracted tether length of 50 ft.

5.2.4. Discussion of Retractor Results

Figure 25 shows spring forces for a 0.015 in coil spring that range from 0.3 to 0.6 lbf, which is satisfactorily close to the original design goal of a constant 0.5 lbf. However, in the simulations of Section 4.1, this designed spring force was found to be far too large for safe operation of the device in microgravity. If retracted 50 ft, even a constant 0.3 lbf force would accelerate the 2.8 lbf gripper to a speed of 18 ft/s, making it a dangerous projectile. Although the spring was thus known to be far too stiff, it was nevertheless used in testing since it was available and served the purposes of characterizing some spring behavior.

Experimentally obtained values for stalled retraction force with the motor ranged from about 1 lbf to 1.4 lbf, which is much lower than the design value of 3.8 lbf. This is not a significant problem for retraction of the gripper, since even a 1 lbf load would accelerate the gripper to 0.5 ft/s within 1 s. A greater force capability may be desired, however, if the system were used for other purposes such as locomotion or payload manipulation. Higher forces would likely be needed for adequate control in these applications. The maximum motor-controlled retraction speed of 0.46 ft/s was well within the 0.5 ft/s safety limit.

The noise observed in the motor force results of Figure 25 was a result of several contributors. Figure 27 illustrates the effect of current limiting the motor voltage supply, which was necessary to protect the motor from thermal overload. When the current limit is exceeded, the supply voltage automatically reduces until the current is within the specified limit. Thus, when the motor stalls, the resulting current surge and overload causes a drop in motor voltage and a subsequent drop in motor current and torque. This combined with the pulsed-field characteristics of the brushless motor resulted in tether tension that peaked quickly after motor stall, and then slowly decayed to a more constant holding force (see Figure 27). Figure 25 shows both the peak forces and the settled

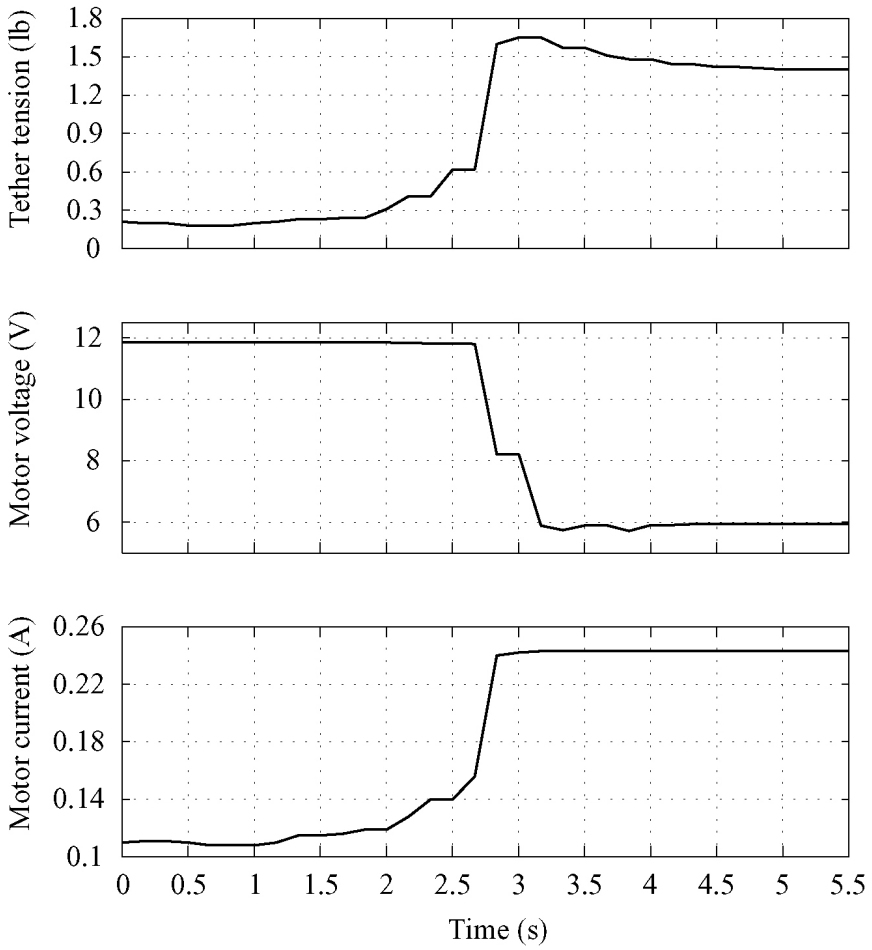

Figure 27. Retractor current-limited stall characteristics at full power.

forces, as reported by the low-pass-filtered visual display of the FUTEK force sensor. The use of a heavily filtered display to record this highly dynamic force also introduced a large amount of noise. However, these values give a good overall representation of the capabilities of the retractor motor system. Another main source of noise in both the spring and motor retraction force measurements was the contribution of static friction between the retractor and the supporting surface. A low-friction bearing surface was used to minimize these effects, as described in Section 5, but remaining static friction contributions were found to be as high as 0.09 lbf.

5.2.5. System Retraction Results

Experimental retraction tests on the air bearing table were a final verification that the original retractor spring designed for the system was far too stiff for safety. The frame sequence shown in Figure 28 shows the gripper being retracted by this spring from the handrail at 0.28 s intervals. Over this retraction distance of only 2 ft, the gripper reached a speed of 2.17 ft/s, which is four times the maximum safe speed for the device.

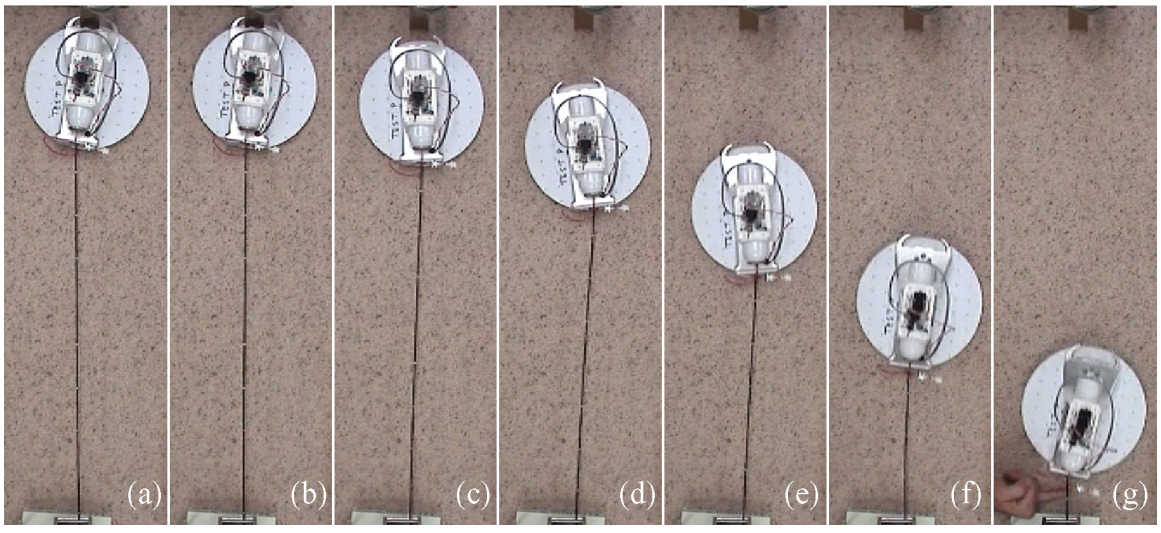

Figure 28. Sequence of spring retraction. Interval between frames is 0.28 s.

Using the video record of the experiment and the known mass of the gripper, an average retraction force of 0.174 lbf was determined for this test. This force is lower than that measured during extension (see Figure 25), but is consistent with forces measured during retraction, as discussed in Section 5.3.2. Figure 29 shows the results of a simulation of this test using the inertial field model of Section 4.1 with initial conditions and spring force measured from the test video. The maximum velocity reached by the gripper in the simulation was 2.24 ft/s, and the schematic representations showing position and orientation of the gripper indicate behavior that is highly similar to that shown in Figure 28. Errors can be attributed to linearization and friction of the spring (described in Section 5.3.2) and use of gripper response on video for calculation of the linearized spring constant.

When tension is applied to the tether as the gripper is released from the handrail, such as under the influence of the spring, unexpected dynamics were introduced that may significantly affect the dynamics of a long tether. Several angular oscillations of the gripper occurred before full release due to the gripper jaw tips alternating contact with the

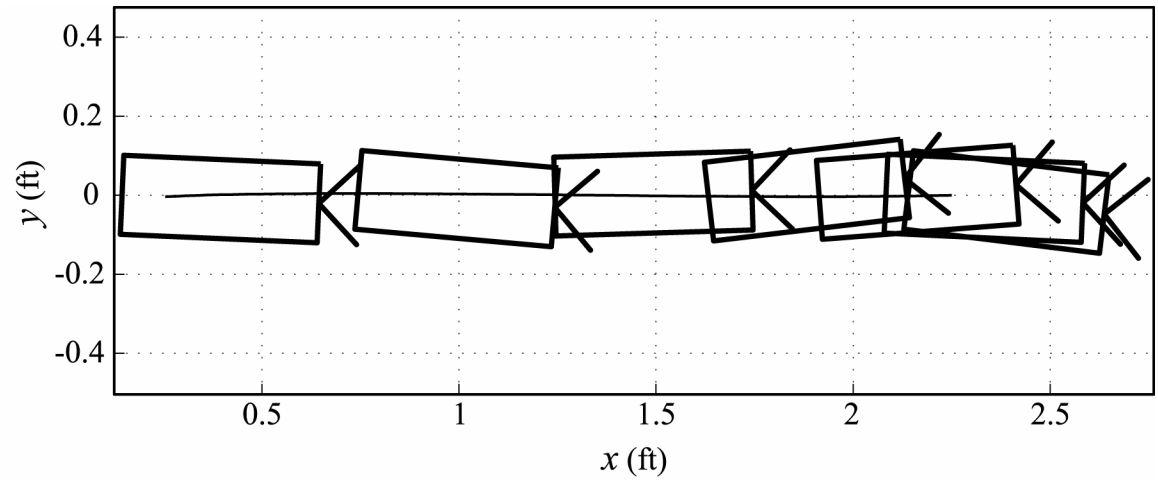

Figure 29. Simulation results of spring retraction with initial conditions similar to those of experimental tests.

backside of the handrail. These oscillations could conceivably produce traveling waves and other vibrations in a tether that is extended to a substantial length. Figure 30 shows the results of maintaining a nominal load of 1 lbf on approximately 2 ft of tether, without any retraction of the tether. In frames (a) and (b), two oscillations with magnitudes of approximately ±2° are shown that took place while the jaws were in the process of opening from the fully closed position. Immediately prior to release, one side of the jaws maintains contact and the gripper is held at an angle of approximately 7° (see Figure 30c and Figure 28a) while the jaws continue opening. Due to this initial angle, rotation is induced in the gripper once it fully releases from the handrail and is retracted, which produces the rotations seen in Figure 28. For the test shown in Figure 30, the end of the tether was held stationary with a tensile load of 1 lbf. Since no retraction device was attached, the gripper was not retracted, and the translation and rotation after release, shown in Figure 30d, is due only to the strain energy stored in 2 ft of tether under a 1 lbf load. Although this exaggerates the resulting rotation of the gripper after release, it is clear that a significant amount of rotation can be brought about by this release behavior. Another interesting result of this test is the amount of movement produced in the gripper

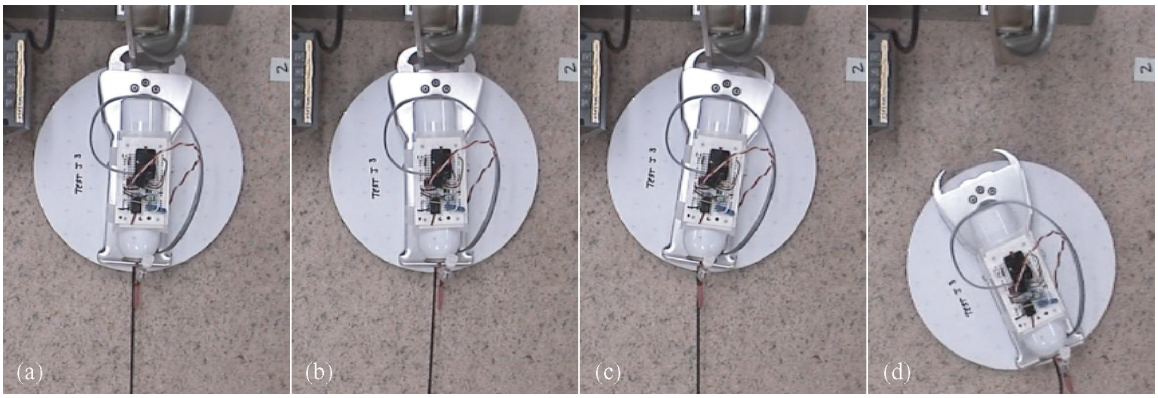

Figure 30. Oscillation and rotation of gripper when released with 2 ft of tether under nominal load of 1lbf.

by releasing the strain energy in the tether. When extended to lengths of scores of feet and released under tension, this longitudinal flexibility of the tether would likely produce important dynamics and must be given attention in future analysis of the tether.

Other forces resulting from tether properties were found to be very significant during the retraction tests on the air bearing table. It was found that the tether tended to retain a portion of the curvature experienced when wound on the retractor reel, and the resulting forces in the tether strongly influenced the behavior of the gripper when retracted at a slower rate. In Figure 31, a sequence of video frames shows a typical motor retraction test with the tether initially slack. Influence of internal tether forces can be seen in frames (a) through (d) in particular, where the gripper undergoes significant rotation induced by the curvature set and stiffness of the tether. Although tests were performed to measure the dynamics introduced by the inner mechanism of the gripper as it released, these forces were dominated by those stemming from the curvature set in the tether and were thus found to be insignificant. These indications of considerable forces

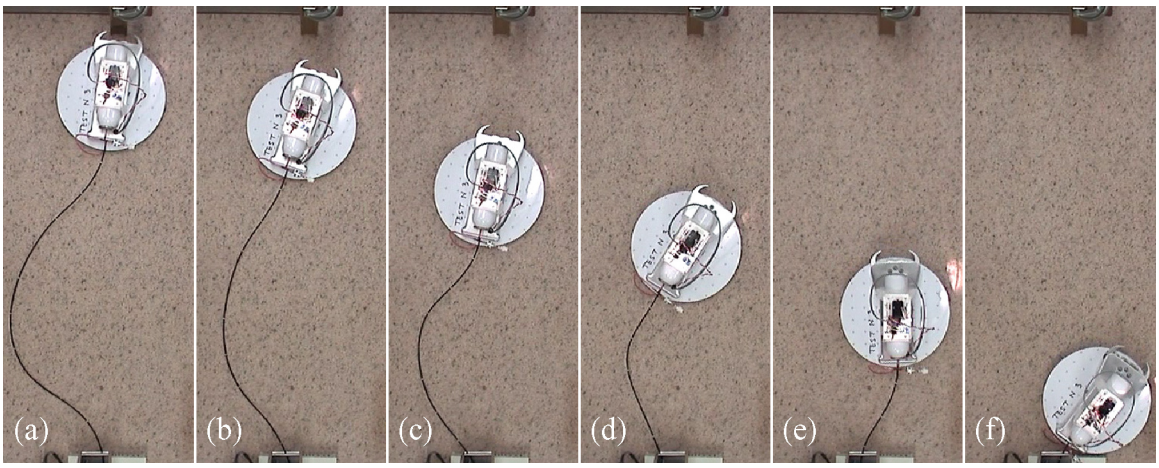

Figure 31. Motor powered gripper retraction test on the air bearing table with the tether initially slack. Interval between frames is 4 s.

from the tether support the conclusions of Section 4.3, which state that inclusion of tether properties is a necessary component of a moderately accurate model of the system.

Other complex dynamics were found to occur during the retractions tests on the air bearing facility. When the gripper was retracted in directions other than along its longitudinal axis, or when forces from the loose tether were sufficient to push it into the anchor, it was often found that the gripper would collide with the anchor. The resulting rebound of the gripper produced significant rotation and translation of the gripper that could potentially have a large effect on its retraction behavior. It was seen in the simulations of Section 4.3 that an initial velocity—linear or angular—of the gripper can greatly affect its behavior during retraction and the conditions of its return to the astronaut. Once the tether is modeled, many initial conditions must be considered and analyzed in order to better understand the behavior of the system under these unpredictable initial conditions.

5.3. General Discussion of Experimental Results

5.3.1. Tether

Some of the most problematic characteristics of the system found during testing were those inherent to the tether itself. It was unexpectedly found that forces internal to the tether had very significant effects on the behavior of the gripper when it is retracted at safe speeds. The main internal characteristic observed, as seen in Figure 31, was a tendency to retain the curvature induced when wound around the retractor reel. This set in the tether is thought to be a result of friction between its composite layers and/or deformation of the urethane jacket and polymer fiber optic casing. Winding on the reel forces the layers of the tether to slide relative to each other, and as the tether is fed and

released from the reel, friction prevents the layers from fully returning to their relative pre-wound positions. These internal forces of the tether were large enough to have a significant effect on the behavior of the gripper when retracted from a distance of 27 in during testing, so if a 50 ft length of this tether were to be used in microgravity, the unpredictable behavior would be unacceptable. The type of tether specified for this system is therefore considered inadequate for this application.

5.3.2. Retractor Spring

Experimental testing verified the results of simulations indicating that the spring implemented for passive retraction is far too stiff for safe operation of the system. Although the original design goal was to emulate the properties of the existing retractable safety tether (see Figure 1b), the two systems are used under different circumstances. The currently used safety tether cannot be remotely released or retracted, and if the hook were ever retracted freely, it would be from a maximum distance of the crewmember's reach, since it must be manually released from an anchor and the retractor is secured to the front of the crewmember's suit. Thus, the 0.5 lbf spring force applied to the existing retractable safety tether serves only to maintain a minimum amount of tether in the workspace when both ends of the tether are secure. When this same load is applied to the free-floating gripper of the automated tether system at any significant distance, the result is dangerous acceleration of a fairly massive object directed toward the crewmember. A spring of thickness 0.007 in was acquired for implementation and testing, but geometric constraints within the retractor precluded its use.

The method of implementation of the coil spring was also found during testing to require redesign. Figure 32 shows the installed spring with the outer coil attached to a

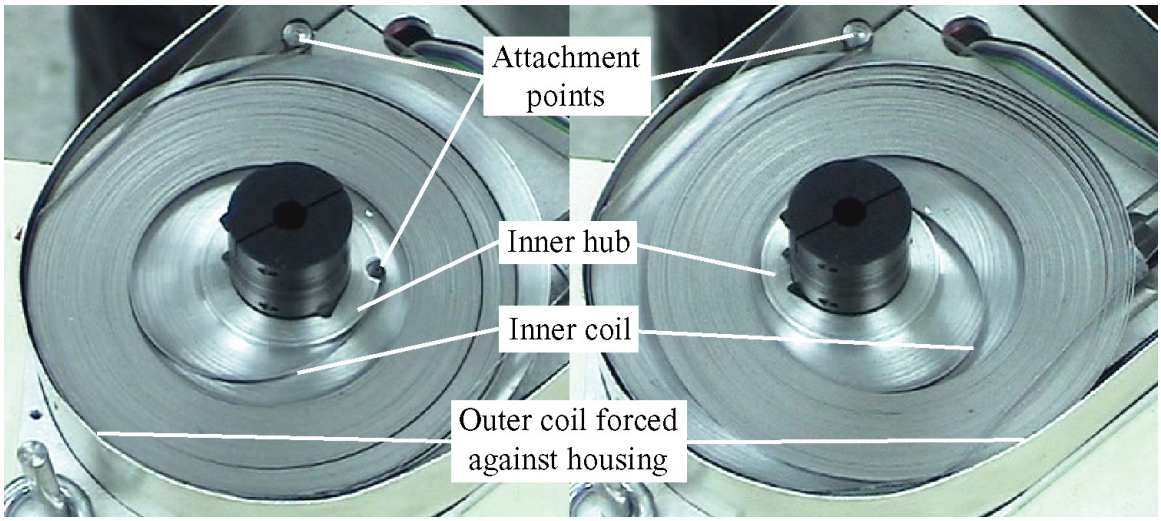

Figure 32. Spring binding against retractor housing

fixed point in the retractor body and the inner coil attached to the inner hub of the reel. During tether retraction, the outermost coils of the spring expand and the inner coil maintains a shape that is as straight as possible within geometric constraints, which forces the outer coil away from the center of the reel in the direction opposite the attachment point on the center hub of the reel. The spring is free to extend beyond the edge of the reel on one side of the retractor (top right in Figure 32), but restricted by the housing midsection on the other (bottom left in Figure 32). Since the inner attachment point of the spring (and thus the direction of outward force on the spring) rotates with the reel, the resulting effect is periodic friction occurring with each revolution of the reel that is often forceful enough to stall retraction completely. The effect of this spring binding is evident in the spring retraction tests of Figure 33, which shows very oscillatory behavior of the force applied to the tether by the spring. This binding problem did not occur while extending the tether against the spring load since the inner coils compressed first and compactly nested against the inner hub of the reel, thus preventing the outer coil from being forced against the inner wall of the retractor body midsection. For this reason, the

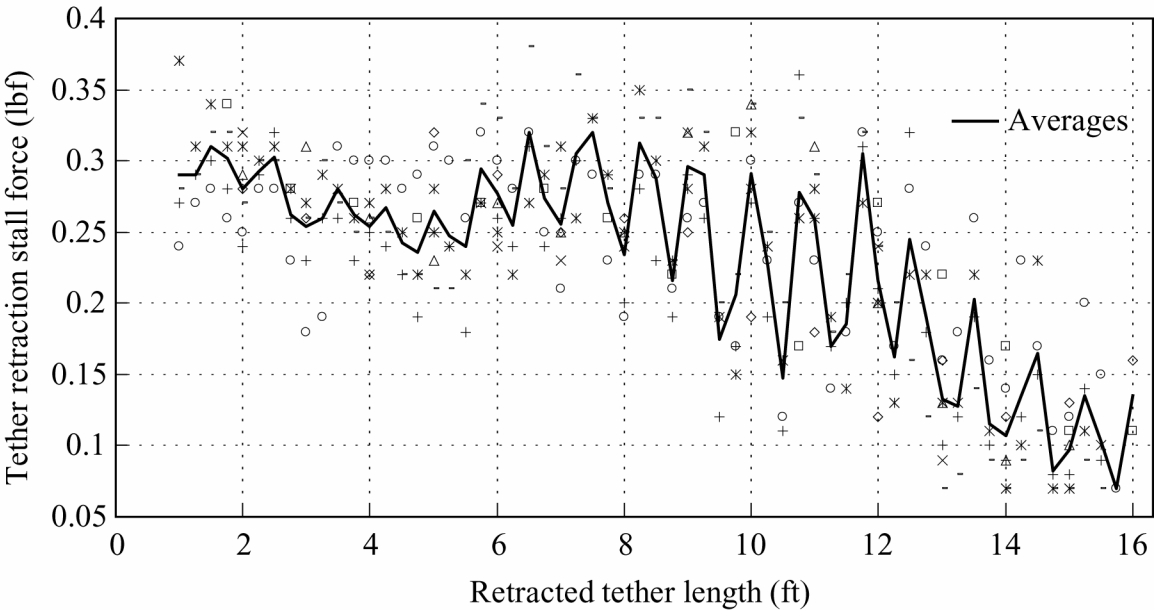

Figure 33. Force profile of spring during retraction. Periodic binding of spring is evident.

measurements of spring retraction forces that are reported in Figure 25 were recorded during extension of the tether.

One potential solution to this problem is forming of the spring steel strip that was used for the spring. The prototype spring was simply a straight length of spring steel wound onto the reel. Since the at-rest shape of the current spring is straight, the inner coil's tendency to return to this shape forces the spring against the retractor housing wall. If the spring were formed into a spiral shape, this force would be reduced, as would the retraction force of the spring, since maximum force for a given thickness of spring is achieved with a maximum stress in the spring. This would be a favorable result, since the force of the current spring is far too great for safety. Another solution that is most likely more effective is a redesign of the attachment method of the spring. If a rim were present on the outer edge of the reel, and the outer coil of the spring were attached to the reel on this outer rim, the outer coils of the spring would be contained therein, preventing friction

with the housing wall. However, since the outer coil of the spring would then be affixed to the reel, the inner coil would require attachment to a point that is fixed and non-rotating relative to the retractor body. This would require a nonrotating shaft to protrude from the center of the reel, which would in turn require a redesign of the active drive mechanism of the retractor, since the current design includes a drive shaft that engages the reel and drives its rotation.

5.3.3. Retraction Actuation

The properties of motorized retraction speed shown in Figure 26 indicate that using the motor for full retraction would be very beneficial for controlling the dynamics of the system. In Section 4.3.3, it was concluded that an optimal retraction method would quickly bring the gripper to a maximum speed, then might accelerate very slightly afterward in order to maintain a small amount of tension in the tether. As shown in Figure 26, the speed of unloaded motorized tether retraction increases as tether is taken onto the reel. The low-speed torque of the motor would quickly accelerate the gripper until the motor's top speed is reached, then as more tether accumulates on the reel, the speed of tether retraction would increase very slowly. This indicates that, with optimization of motor implementation, the active drive of the retractor would provide the best retraction behavior when used for retraction of the entire tether. It may be desirable, then, to dispose of passive retraction altogether and implement only motor-powered retraction. It may still be useful for the spring to engage during tether dispensing in order to limit the amount of tether in the workspace, which is similar to the spring function of the existing retractable tether. This approach would sacrifice additional power consumption for the benefit of favorable retraction characteristics.

6. FUTURE WORK

The purpose of this research was initial exploration of the concept of smart tools, specifically an automated tether system, as a resource for EVA operations. This initial research has provided a great deal of insight into the feasibility and functionality of such a device, but much work must yet be carried out before it can be fully proven as a useful and efficient tool. Following are the main areas of further work that require attention.

6.1. Communications Development

The current research did not address the detailed design or testing of fiber optic communication between the retractor and the gripper, so this subsystem must be finalized and tested. Important issues to address are noise rejection and reliable transmission and interpretation of commands.

6.2. System Improvements

The purpose of the current research is to explore and verify the concept of an automated tether system. For the sake of simplicity, and in order to quickly produce a system that could be used to prove this concept, several of the design requirements listed in Section 2, as well as known shortcomings to the design, were disregarded. These issues, as well as those uncovered during testing, must be addressed in future versions of the system. Other improvements have also been identified that could add significant

functionality to the system and allow broader application. Currently foreseen improvements follow in approximate order of importance.

6.2.1. Tether Modeling and Material

The results of simulations indicate that neglect of the tether in modeling introduces a large amount of error. Although a good deal was learned about the dynamic response of the system under this assumption, details regarding the influence of a tether on that response are noteworthy unknowns. Modeling of a tether is a formidable task, especially when it consists of multiple composite layers that interact statically and dynamically, as in the tether used for the initial prototype system. It is clear that an appropriate tether material must be researched and selected before proper tether modeling can be implemented into the system model.

The tendency of the current tether to retain a portion of the curvature it experiences when wound hinders its usefulness for this application, requiring the use of a different type of tether. One possible solution is a tube of solid material. A hollow center would permit a floating fiber optic core, and a solid, homogeneous tube would prevent curvature presets that arise due to interactions between composite layers. When wound on the 3 in diameter of the retractor reel, the maximum strain experienced by the tether is

$$\varepsilon_{\max} = \frac{d_{teth}}{3in + d_{teth}} \tag{25}$$

where d_{teth} is the outer diameter of the tether. For the 0.118 in tether used for prototyping, this results in a maximum strain of 3.8%, so in order for a solid tube to be a

viable solution, a material must be used for which relatively large amounts of strain remain in the elastic region of deformation.

One material that satisfies this strain requirement is the super-elastic alloy NiTiNOL (Nickel Titanium Naval Ordnance Laboratory). This material has very high kink resistance and at strains of up to 6%, the typical maximum permanent set is a mere 0.2%. The material's high torsional strength would likely be a significant aid in its winding on the retractor reel, but may also introduce undesirable effects such as torsional vibrations. The typical yield strength of Nitinol is sufficient to allow a tube with respective inner and outer diameters of 0.040 in and 0.100 in to bear an axial load of 535 lbf before yielding [15]. According to Equation (25), this outer diameter will then result in a maximum strain of 3.2%, which is well within the super-elastic region of deformation for this material. This type of tether will likely also introduce a certain amount of buckling strength, particularly at smaller lengths of tether extension, which would likely significantly affect the behavior of the free-floating gripper during retraction and must be examined.

One unusual property of Nitinol is that of shape memory. Its material properties are controlled by a transformation temperature below which it is easily plastically deformed and above which it will return to its pre-deformed shape, even in the presence of very high opposing forces. This transformation temperature of Nitinol can vary widely with different alloys and heat treatments with typical values that range between -60°F and 330°F [16], and may in principle be reduced to approximately -150°F or below. In order to be usable as a tether material, a Nitinol alloy would be required to have a transition temperature at or below -220ºF in order to possess super-elastic properties during

temperature verification tests of EVA hardware. This is due to the fact that the super-elastic properties mentioned above are characteristic of Nitinol alloys when maintained at approximately 120°F above the transformation temperature [17] or higher, so another potential challenge of this approach would be to design an alloy for which the super-elastic properties are dominant over the extreme range of temperatures found in space (-200°F to +250°F). However, the potentially high forces that can be applied by Nitinol when used as a shape memory alloy may also be useful in conjunction with a device such as the automated tether system in certain applications.

One property of a super-elastic alloy tether that may be undesirable is longitudinal flexibility. When a tensile force is applied, the super-elastic material would behave as a long spring. This would be beneficial for reducing the impact of impulse loads, but when the potential energy thus stored in the tether is returned to external components in the form of kinetic energy, situations may be introduced that are more dangerous than the cause of the original impulse load. Special provisions would also be required to protect the less flexible fiber optic core.

Although there are many favorable tether properties of super-elastic alloys such as Nitinol, it is clear that a careful analysis is required to determine the suitability of this type of material for an automated tether management system. Tether properties must be analyzed along with feasible retraction methods to determine the optimal configuration.

Another tether property worthy of consideration is electrical conductivity. While it is undesirable to use long conductors on orbit for control of electrical signals, a conductive tether may be useful for neutralizing electrical potential differences between objects at the ends of the tether. If an astronaut were working at the end of a non-

conducting tether without any other physical contact with the anchoring spacecraft, a static potential could build up on the exterior of the astronaut's suit relative to that of the spacecraft, which would be abruptly neutralized upon contact with the spacecraft. The electrical pulse resulting from this neutralization could potentially damage electronics or have other undesirable effects. For this reason, the need for electrical conductivity must be explored during selection of the appropriate tether material.

6.2.2. Retraction Methods

The optimal methods of retraction must be determined. Thus far, passive spring retraction was found difficult because without velocity damping, gripper speeds grew too large. When damped, the decreasing force from the relaxing spring caused retraction of the tether to slow and the gripper to overtake the tether, which in turn caused an increase in the lateral drift of the gripper as it reached the astronaut when in orbit. One solution to this problem is to use motor retraction exclusively, as described in Section 5.3.3, which details the beneficial properties of motorized retraction. However, this approach requires much higher power consumption. Since passive retraction is preferable from this standpoint, research should be conducted to determine the feasibility of a passive solution that will produce the desired retraction properties described in Section 4.3.3.

Another element of retraction control that is worthy of investigation is implementation of a small propulsion system on the gripper. For an object floating freely in microgravity, gas propulsion is the only current method of total position, speed, and orientation control. With such a propulsion system, full control of the gripper during retraction would theoretically be possible, which would allow unlimited retraction distance and optimal retraction times with perfect positioning and speed upon return to

the astronaut. The cost of these advantages is extensive additional hardware, more complex control algorithms, and an additional type of energy storage. Required hardware would include valves, jets, propellant storage, and gyroscopes and other sensors, which would significantly increase the minimum size of the gripper. In addition, a compressed gas supply would require regular monitoring and replenishment.

6.2.3. Reduction of Moments at Anchor

When the gripper is engaging an anchor with a firm grip, large moments can be introduced to the anchor, depending on the direction of tether tension relative to the gripper. This can also occur with a loose grip on the handrail, since little rotation of the gripper is possible. On the current gripper prototype, 8 in separate the point of contact with the anchor and the end of the handle where the tether is attached. Any component of force on the tether normal to the longitudinal axis of the device would translate through the rigid handle to a moment and force on the gripped anchor. This is potentially very damaging to both the gripped object and the gripper jaws. Standard EVA handrail is rated for a maximum 300 in-lbf moment acting simultaneously with a 50 lbf force in any direction, so in a worst case of the tether being pulled perpendicular to the handle, only a 37 lbf tether load would be permissible within the handrail rating. This problem is complicated by the requirement of the gripper to incorporate a handle, which places a minimum limit on the permissible length of the device. Therefore, a pivot point that allows the handle to rotate or other solution that reduces this moment arm should be implemented into the mechanical design of future versions.

6.2.4. Full Conformity to EVA Tool Requirements

In order to be acceptable as an EVA tool, the system must conform to all requirements established by NASA for EVA tools [3]. The main features that the current system lacks in this area are a redundant gripper safety lock and improved battery implementation for both devices.

All safety tether hooks are required to implement a redundant lock that precludes accidental release. In the case of the gripper, the non-backdrivability of its lead screw provides passive mechanical locking, but accidental motor activation would still move its jaws. An evaluation must be conducted to identify what possible measures would provide appropriate redundant locks in this case. Possibilities include mechanical shields of controls or requiring simultaneous activation of multiple controls.

Battery-powered EVA tools are required to allow for a suited crewmember to replace the batteries at the EVA worksite. For design simplicity, the current automated tether system requires disassembly of both the gripper and retractor in order to replace their respective batteries. Another required battery-related feature that is absent on the current system is an indicator that displays the level of battery charge. These issues are relatively simply solved by implementing a battery access door and adding the electronics and indicators necessary for battery status display.

6.2.5. Manual Gripper Operation

In the event of unexpected power loss or other contingency, the gripper must be capable of manual operation. An interface should be implemented to allow a suited astronaut to manually operate the gripper. This manual operation must be designed such

that accidental manual operation is precluded while being relatively easy to operate in the event of a contingency.

6.2.6. Polymeric Gripper Jaw Coating

Although the prototype gripper jaws are solid aluminum, the intent of their design was implementation of a polymeric coating for distribution of pressures applied to an anchor and protection of both jaw and anchor from marring and burring. In particular, the inner protrusions of the jaws were intended to consist of a stiff yet deformable material that would conform to anchors. Future revisions of the system must incorporate some type of jaw coating or other method of protecting anchors from dangerous burring and marring.

6.2.7. Communications

Although the initial design of the fiber optic communication system incorporates a single channel, two-way communication between the gripper and retractor would be very beneficial and should be investigated as the communications system is developed and optimized. This would allow monitoring of system status, such as speed and applied force, and would allow control of the system from user interfaces on either the gripper or retractor. With these additions, more diverse applications would be possible, such as cargo manipulation or crewmember locomotion (see Section 6.3). Bidirectional communication can be accomplished in fiber optics with either a pair of single-mode fibers with each dedicated to a particular direction of communication, or a single bifurcated fiber that allows both transmission and reception of communication along the same fiber. Bifurcated fiber would not allow simultaneous transmission and reception of communications, but the advantage of using a single fiber may outweigh this drawback

for certain control schemes. More advanced communication features such as voice command and computer interfacing may also be of interest in future versions of the system.

6.3. Parallel Manipulation and Other Applications

The automated features of the automated tether system provide for potential use in a variety of applications other than that of a safety tether. A high degree of adaptability has already been incorporated, and multiple versions of the system are conceivable with specializations for specific applications. The main applications considered so far are cargo manipulation and crewmember locomotion.

If used for manipulation, multiple, synchronized tether systems would be necessary for proper control of a payload. Two tether systems in an antagonistic configuration could control the position of a payload along a line. Three systems can control translation within a plane, and six systems could theoretically fully control position and orientation in three dimensions. The advantage of such a system is large savings of space, launch weight, and power consumption over traditional robotic serial manipulators. An outer framework would be required for support of the tethers, which may be relatively compliant and delicate. Hybrid manipulation is also an option, in which one or more traditional serial manipulators are used in conjunction with the tether systems and provide a portion of the required support. Control algorithms would be required that include optimal tether distribution across existing supporting structures in order to protect the integrity of the supports, provide maximum maneuverability, and prevent tether crossover. Hardware that allows communication and synchronization between several automated tether units would also be necessary. If tether-based

manipulation were proven valuable, a supporting structure may even be implemented specifically for the tether system that would support expected loads in an optimal configuration.

Crewmember locomotion is another potential use of the automated tether system. Safety is a major concern when a suited crewmember is in motion in any context, so control algorithms must be developed accordingly. When pulled in a given direction with a single tether, minimal control of the crewmember is possible, but two antagonistic systems could likely provide sufficient control along a line. If a long-term travel corridor were convenient across an open space of a structure, for example, this type of configuration could provide safe transportation.

7. CONCLUSION

An automated tether management system has been designed, simulated, and tested for the purpose of increasing efficiency of valuable EVA time. The system consists of a remotely releasable, self-locking robotic gripper that engages a variety of anchors; a retractor with both passive and active actuation capability that contains and controls the length of tether in the workspace; and a hybrid tether with tensile structural support capability and a fiber optic core to allow communication between the retractor and the gripper. The system is designed to conform to NASA standards for safety tethers [3] and expand the role of the currently used retractable safety tether.

Simulations of the system show that on-orbit coriolis effects limit the allowable length of tether, and that retraction methods for the retractor require further analysis. Further modeling is needed, however, in order to better understand the dynamics of the system. Current modeling methods neglected dynamics of the tether for simplicity, but results indicate that a significant amount of error was introduced thereby.

Experimental results verified applicable simulations, and quantified the capabilities of the system, which were found in general to be sufficient for the role of a safety tether. During experimentation, it was found that the tether chosen for the prototype system was inadequate for the current application due to the curvature sets induced by winding onto the reel of the retractor. Further research is needed to determine an appropriate tether material.

Properties of the system indicate many more applications than a personal safety tether, and indicate the possibility of specialized versions of the system for specific applications. Multiple tethers can be used simultaneously for payload manipulation, and motorized retraction could be used as a method of crewmember locomotion.

Although more work must be accomplished before the automated tether system can be a useful tool, the current research provides important groundwork for further development of such a system. With the knowledge gained during this research, all elements of the system can be concurrently modeled, designed, and optimized to result in a next-generation prototype with functionality near to that required for tools used in space.

REFERENCES

[1] Rochlis, J., Discussions with, Robotics and Automation Division, NASA Johnson Space Center, Houston, Texas. jennifer.l.rochlis1@jsc.nasa.gov, 2002.

[2] Mission Operations Directorate, EVA Robotics and Crew Systems Operations Office. (2001, May). Online EVA Tool Catalog. [Online]. Prepared by R. C. Trevino and R. K. Fullerton. Available: www4.jsc.nasa.gov/org/df42/evatoolcatalog/index.htm.

[3] EVA and Crew Equipment Projects Office, "Extravehicular Activity (EVA) Hardware Generic Design Requirements Document," Prepared by D. S. Adlis. NASA Doc. No. JSC-26626A. 1995.

[4] Mission Operations Directorate, "EVA Tool Catalog," Prepared by R. C Trevino and R. K. Fullerton. NASA Doc. No. JSC-20466. 1985.

[5] Cobb, J., Discussions with, P.O. Box 330, Cortland, New York, (607)753-8276. 2001.

[6] Mahalingam, S.S., M.; Dwivedi, S.N.; Vranish, J.M., "Special challenges of robotic gripping in space," in *System Theory, 1988., Proceedings of the Twentieth Southeastern Symposium on*, 1988, pp. 581-586.

[7] Biagiotti, L., C. Melchiorri, and G. Vassura, "Position/force control of an arm/gripper system for space manipulation," in *2001 IEEE/ASME International Conference on Advanced Intelligent Mechatronics Proceedings*, 2001, vol. 2, pp. 1175-1180.

[8] Arisumi, H. and K. Komoriya, "Catching motion of casting manipulation," in *2000 IEEE/RSJ International Conference on Intelligent Robots and Systems*, 2000, vol. 3, pp. 2351-2357.

[9] Arora, J.S., *Introduction to Optimum Design*, New York: McGraw-Hill, 1989.

[10] D'Souza, A.F. and V.K. Garg, *Advanced Dynamics: Modeling and Analysis*, Englewood Cliffs, NJ: Prentice-Hall, 1984.

[11] Wells, D., Discussions with, Robotics and Automation Division, NASA Johnson Space Center, Houston, Texas. dennis.l.wells1@jsc.nasa.gov, 2002.

[12] Falcon Safety Products. (2003, Feb.). Dust-Off Product Web Site. [Online]. Dust-Off Product Web Site. Available: www.falconsafety.com/ dust_off/index.html.

[13] Choset, H., R. Knepper, J. Flasher, S. Walker, A. Alford, D. Jackson, D. Kortenkamp, R. Burridge, and J. Fernandez, "Path planning and control for AERCam, a free-flying inspection robot in space," in *Proceedings of the 1999 IEEE International Conference on Robotics and Automation, ICRA99*, 1999, vol. 2, pp. 1396-1403.

[14] Akin, D., Discussions with, Dept of Mechanical Engineering, University of Maryland. 2002.

[15] Matweb.com. (2003, Mar.). Nitinol - NiTi Shape Memory Alloy; High-Temperature Phase. [Online]. Nitinol - NiTi Shape Memory Alloy; High-Temperature Phase. Available: www.matweb.com/search/Specific Material.asp?bassnum=MTiNi0.

[16] Lin, R. (2003, Mar.). Shape Memory Alloys and Their Applications. [Online]. Shape Memory Alloys and Their Applications. Available: www.stanford.edu/~richlin1/sma/sma.html.

[17] Nitinol Devices and Components. (2003, Mar.). Nitinol Technology. [Online]. Nitinol Technology. Available: www.nitinol.com/3tech.htm.